International
Progress Report

IPR-03-37

Äspö Hard Rock Laboratory

Update of the rock mechanical model 2002

Hossein Hakami
Itasca Geomekanik AB

December 2003

Svensk Kärnbränslehantering AB
Swedish Nuclear Fuel
and Waste Management Co
Box 5864
SE-102 40 Stockholm Sweden
Tel 08-459 84 00
+46 8 459 84 00
Fax 08-661 57 19
+46 8 661 57 19

Äspö Hard Rock Laboratory

Report no.
IPR-03-37
No.
F117K
Author
Hossein Hakami
Date
Dec.2003
Checked by
Rolf Christiansson
Date
2005-06-03
Approved
Christer Svemar
Date
2005-06-07

Äspö Hard Rock Laboratory

Update of the rock mechanical model 2002

Hossein Hakami
Itasca Geomekanik AB

December 2003

Keywords: Äspö site descriptive model, GeoMod, Rock mecanics, In-situ stress, Fracture zones, Numerical analysis, 3DEC, Principal stress, Spatial

Preface

The main purpose of the GeoMod project, which initiated in the beginning of 2002, was to update the previous geoscientific model of Äspö (Äspö96), mainly by incorporate additional data collected after 1995. The updated model (Äspö02) was meant to, as far as possible, be integrated in a three dimensional digital model and to be documented in a single technical report.

The geoscientific disciplines: geology, rock mechanics, hydrogeology and hydrogeochemistry, were supposed to be integrated into a common understanding of the site. However it became obvious, during the spring 2003, that the necessary integration efforts far exceeded the expected. As a result of this, the GeoMod project was temporarily terminated in May 2003. SKB consider taking up the project again during 2005.

The result obtained within rock mechanic, when the project was terminated, is presented in this report. The other progress reports are:

- IPR-03-34
  Äspö Hard Rock Laboratory
  Update of the geological model 2002

- IPR-03-35
  Äspö Hard Rock Laboratory
  Update of the hydrogeological model 2002

- IPR-03-36
  Äspö Hard Rock Laboratory
  Update of the hydrogeochemical model 2002

Recommendations of further work are presented in the reports.

The helpful comments, suggestions and reviewing from Johan Andersson, Mel Cascoyne, Richard Everitt, John A Hudson, and Bill Lanyon are acknowledged. The support and help from: Mansueto Morosini, Tommy Olsson and Roger Taringer are acknowledged.

Rolf Christiansson

Abstract

Alongside the commencement of site-specific characterization of candidate sites, need for site descriptive models have been apparent. The present work describes how numerical analyses performed by the distinct element program 3D may be employed in order that a forecast of the spatial distribution of in-situ stresses is made.

At a site, where an underground facility is planned, the in-situ stresses are commonly determined by a number of measurements carried out in few boreholes, sparsely sunk into the rock formation. The stresses data are very local information and do not explicitly reflect the effect of large discontinuities crossing the rock formation in question. It is well known that those discontinuities largely influence the state of stress, especially in closer neighbourhoods. The major fracture zones are, therefore, re-constructed numerically in the 3DEC models performed and are exposed to loading in shear, upon which the in-situ stresses change, more pronounced close to the zones and just slightly at a distance.

The first part of the numerical investigations concerned the HQ3-area. The area lent itself for numerical analysis, as a detailed structure geological characterization was already available. While the central part of the numerical block included accurately the structures (moderately large fracture zones and single, dominant fractures), five regional fracture zones were also incorporated in the numerical model block, which extended over a volume of rock $4.4 \times 4.4 \times 4$ km in size.

To perform numerical analyses, involving the GeoMod block, composed the second part of the investigations. A virtual rock block, having the size of $1 \times 1 \times 1$ km, designated as the GeoMod block was selected out of the Äspö area, within which the findings from four parallel investigations were to be collected and demonstrated. The disciplines associated with the parallel investigations were structure geology, geochemistry, geohydrology and rock mechanics.

A total number of nine regional and major fracture zones were incorporated in the numerical model block. Analyses performed depicted a spatial distribution of in-situ stress within the GeoMod block.

Following the confirmation, made by continued structure geological investigations, that some of the fracture zones tapered off towards the deep ends, improvement was made to the way fracture zones were numerically modelled.

The analyses show that the stress tensor rotates, as the observation point gets closer to a major structure. All three principal stresses, σ_1, σ_2, and σ_3 vary in magnitude and orientation. The orientation of σ_1, however, does not deviate along its trajectory more than about ten degrees even though the point of observation is in the vicinity of a major structure.

The other two components of principal stress tensor, σ_2, and σ_3, tend to rotate considerably near the crest of prismatic rock parties delimited by the major fracture zones, to the extent that they may replace each other under a certain depth interval.

Sammanfattning

I samband med att arbete med platsundersökningar påbörjats har behovet av metoder för platsbeskrivande modeller blivit uppenbart. Denna rapport beskriver hur numeriska analyser gjorda med beräkningsprogrammet 3DEC, kan användas som ett verktyg för att förstå och prognostisera rumslig variation i bergspänningar *in-situ*.

Vid planeringen av en berganläggning brukar man normalt utföra bergspänningar i några punkter i enstaka borrhål. Mätdata bli därför mycket lokal information och speglar inte nödvändigtvis de effekter av större strukturer som kan finnas i området i fråga. Det är känt att de större sprickzonerna kan inverka på spänningsfältet, i synnerhet i dess närhet. Större zoner har därför inkluderats i uppbyggda 3DEC-modeller. Sprickzonerna modelleras som plan med svagare egenskaper än omgivande berg och utsätt för belastning. På detta sätt simuleras det verkliga spänningsfältet och de spänningsvariationer som uppkommer på grund av rörelser i modellen är störst vid zonerna och mindre på ett längre avstånd från dem.

Den första delen av numeriska modelleringen gällde ett område kallat HQ3. Detta område studerades eftersom en detaljerad geologisk karakterisering och spänningsdata fanns tillgängligt. Den centrala delen av den numeriska modellen innehåller såväl medelstora sprickzoner som ett fåtal större enskilda dominerande sprickor. Därutöver var fem regionala zoner inkluderade, vilka sträckte sig genom ett block av 4.4 × 4.4× 4 km storlek.

Den andra delen av modelleringen gällde att studera det så kallade GeoMod-blocket, som är ett 1 × 1 × 1 km stort område valt omkring Äspö-laboratoriet. I detta block skulle modeller inom fyra olika ämnesområden, strukturgeologi, geokemi, geohydrologi och bergmekanik, parallellt tas fram och metoder demonstreras. Den numeriska modell som analyserats inkluderade nio större sprickzoner. Resultaten visar på förväntat spänningsfält inom det studerade GeoMod-blocket.

Efter att de strukturgeologiska undersökningarna visat att några av sprickzonerna smalnade av mot djupet, förbättrades den numeriska modellen så att sprickzonerna blev simulerade på ett motsvarande sätt.

Beräkningarna visar att huvudspänningarna roterar då observationspunkten ligger nära en större sprickzon. Alla tre huvudspänningar får en förändrad magnitud och riktning. Den största huvudspänningens riktning varierar dock som mest upp till ca 10 grader även i närheten av en större struktur. De andra två huvudspänningarna roterar avsevärt i vissa områden som avgränsas av sprickzoner och för vissa djup byter den minsta huvudspänningen riktning med den intermediära.

Contents

1 Introduction

The Swedish Nuclear Fuel and Waste Management Company (SKB) established the Äspö Hard Rock Laboratory in late 1980th in order serve as a test area for SKB's work to design and construct a deep geological repository for spent fuel and to develop and test methods for characterization of selected repository site.

The role of the Äspö Hard Rock Laboratory is to provide input to the performance assessments that have to be supplied as part of each license application and to develop, test, and evaluate methods for site investigations, detailed investigations, repository construction as well as disposal and backfilling of tunnels before they are applied within the deep repository programme. The work with the Äspö HRL has been divided into three phases: the pre-investigation phase, the construction phase, and the operating phase.

During the Pre-investigation phase, 1986–1990, studies were made to provide background material for the decision to locate the laboratory to a suitable site. The natural conditions of the bedrock were described and predictions made of geological, hydrogeological, geochemical etc conditions to be observed during excavation of the laboratory. This phase also included planning for the construction and operating phases.

During the Construction phase, 1990–1995, comprehensive investigations and experiments were performed in parallel with construction of the laboratory. The excavation of the main access tunnel to a depth of 450 m and the construction of the Äspö Research Village were completed. Excavation started on October 1st, 1990 after approval had been obtained from the authorities concerned, and was completed in February 1995.

At the end of the construction stage, the different models used during the site characterization were compiled and evaluated as a first attempt to establish a multidisciplinary site descriptive model, where the results were published in a series of technical reports:

- Stanfors, R, Erlström, M, Markström I. Äspö HRL – Geoscientific evaluation 1997/1. Overview of site characterization 1986 – 1995. SKB TR 97-02.
- Rhen, I (ed), Bäckblom G., Gustafson, G, Stanfors, R, Wikberg, P. Äspö HRL – Geoscientific evaluation 1997/2. Results from pre-investigations and detailed site characterization. Summary Report. SKB TR 97-03.
- Stanfors, R, Olsson, P, Stille, H. Äspö HRL – Geoscientific evaluation 1997/3. Results from pre-investigations and detailed site characterization. Comparison of predictions and observations. Geology and Mechanical stability. SKB TR 97-04.
- Rhen, I, Gustafson, G, Wikberg, P. Äspö HRL – Geoscientific evaluation 1997/2. Results from pre-investigations and detailed site characterization. Comparison of predictions and observations. Hydrogeology, Groundwater chemistry and Transport of solutes. SKB TR 97-04.

- Rhen, I (ed.), Gustafson, G, Stanfors, R, Wikberg, P. Äspö HRL – Geoscientific evaluation 1997/2. Models based on site characterization 1986 – 1995. SKB TR 97-05.

- Almén K-E (ed), Olsson P, Rhen I, Stanfors R, Wikberg P. Äspö Hard Rock Laboratory. Feasibility and usefulness of site investigation methods. Experience from the pre-investigation phase. SKB TR 94-24.

The Operating phase began in 1995. A preliminary outline of the programme for the Operating phase was given in SKB's Research, Development and Demonstration (RD&D) Program 1992. Since then the programme has been revised and the basis for the current programme is described in SKB's RD&D Program 1998.

During the operating stage a number of different experiments and studies have been executed in Äspö HRL, which provides additional information compared to the experience obtained and presented in the previous reports. In order to update the geoscientific models, SKB initiated the project GeoMod to compile the results from the operating period 1995-2002.

1.1 The GeoMod project

1.1.1 Objectives

The GeoMod project was aiming at updating the existing model by integrating new data collected since 1995. The major part of the new data has been produced in the lower part of the Äspö tunnel spiral. The updated model is contained in a 1 km^3 cube with focus on a volume including the tunnel spiral volume from about –200 metres to about –500 metres.

The specific objectives in the GeoMod project were to:

- Describe the geoscientific properties of a prescribed rock volume containing the tunnel spiral.
- Identify relevant processes to explain the geoscientific properties.
- Define the boundary conditions of importance to the rock volume processes.
- Develop methodology to integrate the knowledge from the different geoscientific disciplines.
- Develop a coherent integrated geoscientific model of Äspö.

The project started January 2002. Before the integration of the models finished the GeoMod project was temporarily terminated in May 2003. Finally, SKB decided to reduce the content of the project by omitting the fully integration between the different geoscientific disciplines. It was decided that the work with the completed integration was postponed until 2005.

As a consequence, the different geoscientific models; i.e. geological, hydrogeological, rock mechanics and hydrogeochemical, are published in four separate reports, one for each discipline.

The objectives of this report are to present the result within rock mechanics.

1.1.2 This report and other GeoMod related reports

This report presents the updating of the rock mechanics part of the GeoMod project.

Three other reports are produced within GeoMod:

- IPR-03-34
  Äspö Hard Rock Laboratory
  Update of the geological model 2002
  Johan Berglund, Philip Curtis, Thomas Eliasson, Tommy Ohlsson, Peter Starzec, Eva-Lena Tullborg
  December 2003

- IPR-03-35
  Äspö Hard Rock Laboratory
  Update of the hydrogeological model 2002
  Patrik Vidstrand
  December 2003

- IPR-03-36
  Äspö Hard Rock Laboratory
  Update of the hydrogeochemical model 2002
  Marcus Laaksoharju, Ioana Gurban
  December 2003

1.1.3 Reviewing

Although, a complete integration between the disciplines was not accomplished in the current version of the geoscientific modelling, the relation and interaction between the disciplines were addressed with respect to the scientific content. The Scientific Content Issues are:

- Is the scientific content complete, given the objectives and current level of the work?
- Is the science clearly explained?
- Is the model adequate?
- Is it clear how updating can be accomplished?
- Is the presented information traceable?
- Are the conclusions justified and adequate?
- Confidence in the model and robustness

The evaluation and the robustness for the different disciplines have been in focus and the statements put forward in the individual reports are not contradictive unless this is clearly stated.

2 Site location and overview of existing data

2.1 Overview

The Äspö HRL is located on the Äspö Island, which is located near to the Simpevarp nuclear site. A great number of investigations have been made both on Äspö and in adjacent areas, such as Laxemar and Ävrö, c.f. Figure 2-1.

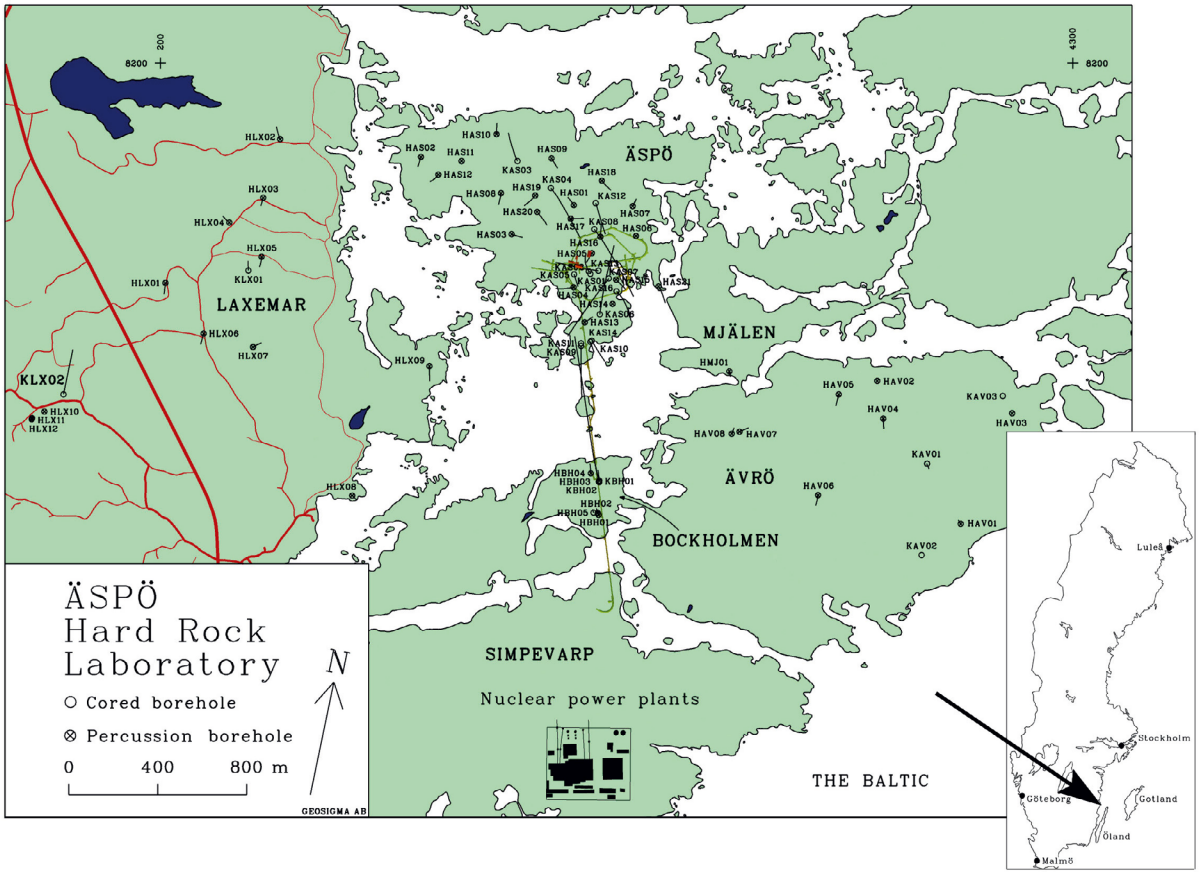

Figure 2-1. *Overview of the Äspö Island and the adjacent areas. The selected model domain is shown in Figure 2-2.*

The GeoMod-project will update the existing model by integrating new data collected since 1995. Most new data have been collected during the operational phase for different experiments conducted in the tunnel. The majority of the new information originates from the experimental sites in the lower part of the Äspö HRL. The updated model will focus on a volume including the tunnel spiral (c.f. Figure 2-2.).

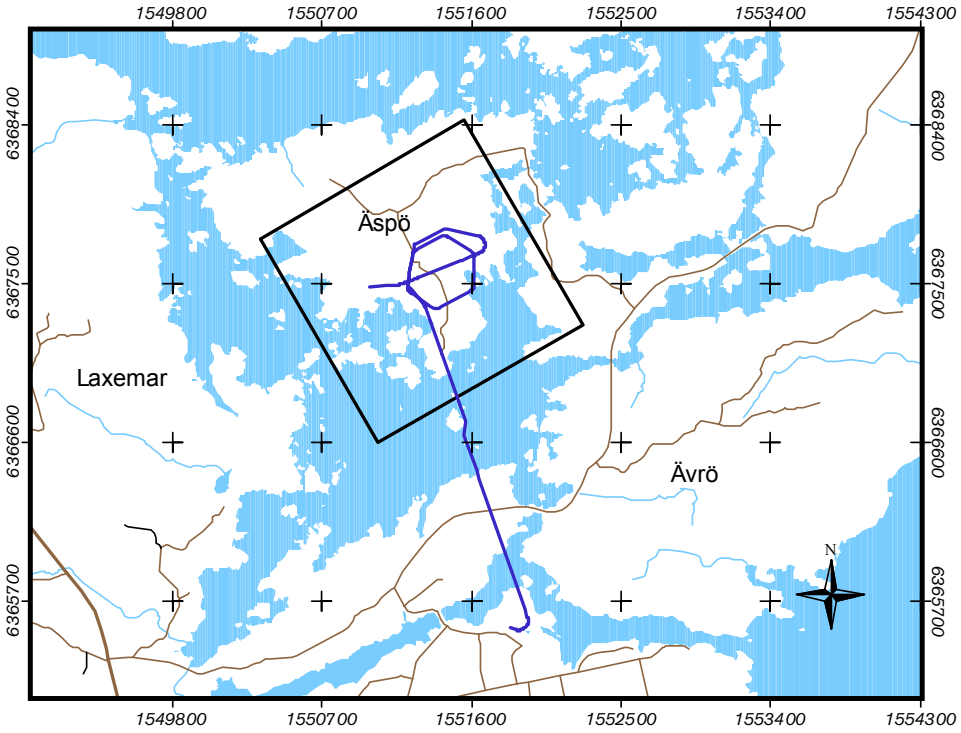

Figure 2-2. *Map showing the GeoMod model area along with the horizontal projection of the Äspö tunnel (RT90 coordinate system).*

2.2 Co-ordinate system

The virtual cube with following corner coordinates defines the corner coordinates of the model volume.

Table 2-1. Model volume coordinates.

Äspö 1km Cube Coordinates			
RT90-RHB70			
	Easting	Northing	Elevation
	[m]	[m]	[m]
Top square			
1	1551200.046	6367099.181	50
2	1550700.046	6367965.206	50
3	1551566.071	6368465.206	50
4	1552066.071	6367599.181	50
Bottom square			
5	1551200.046	6367099.181	-1000
6	1550700.046	6367965.206	-1000
7	1551566.071	6368465.206	-1000
8	1552066.071	6367599.181	-1000

The modelling is contained within a common virtual cube with 1 km side length extending from +50m to -1000 mamsl (meter above mean sea level) in elevation to which appropriate boundary conditions have to be set. This volume is to be tied to its regional context based on the previous model, Äspö96.

2.3 Geoscientific investigations and experiments made

The underground part of the laboratory consists of a tunnel from the Simpevarp peninsula to the southern part of Äspö where the tunnel continues in a spiral down to a depth of 450 m (Figure 2-3). The total length of the tunnel is 3600 m where approximately 400 m at the end have been excavated by a tunnel-boring machine (TBM) with a diameter of 5 m. The first part of the tunnel has been excavated by conventional drill and blast technique. The underground tunnel is connected to the ground surface through a hoist shaft and two ventilation shafts. Äspö Research Village is located at the surface on the Äspö Island and it comprises office facilities, storage facilities, and machinery for hoist and ventilation (Figure 2-3).

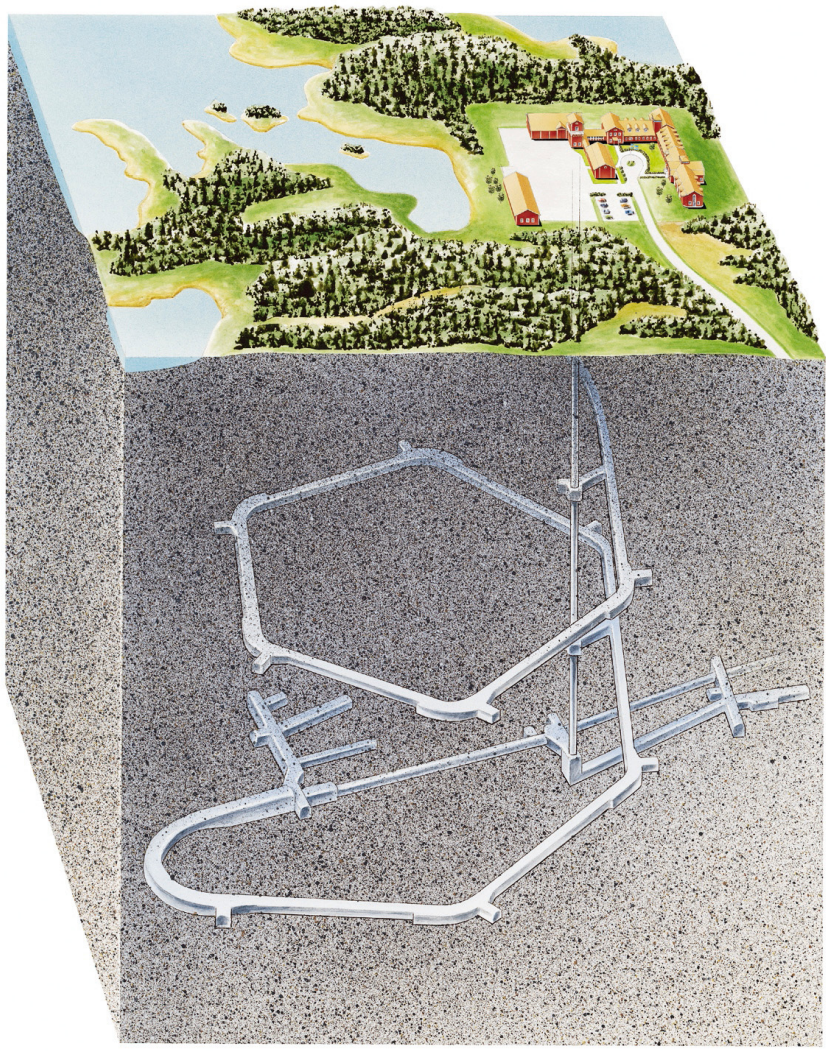

Figure 2-3. *Overview of the Äspö Hard Rock Laboratory Facilities within GeoMod virtual volume.*

2.3.1 The data used in the modelling

All data used for the modelling were quality assured data, received from SKB database SICADA. The database contains all tests, sampling and analyses obtained from percussion and core drilled boreholes at surface or in the underground experimental areas of Äspö HRL.

2.3.2 Experiments in Äspö HRL

A great number of experiments have been executed in Äspö HRL since the start of the operating phase. Examples of experiments where relevant data was collected are e.g., REX, TRUE, TRUE BS, HQ, ZEDEX, JADE, MICROBE, COLLOID, PROTOTYPE REPOSITORY, MATRIX and other experiments.

3 Previous Äspö Models

Formally, the work presented in this report is an update of the rock mechanical investigations that were reported in "Äspö HRL – Geoscientific evaluation 1997/5, Models based on site characterization 1986-1995" by /Ingvar Rhen et al., 1997/. The rock mechanics model, presented in that work was based on three domains:

- The state of in-Situ stress.
- The mechanical properties of rock masses within Äspö area.
- Classification of rock masses found within the area in question.

The current work, however, even though in part related, was not directly erected on the outcome of the investigations reported by /Rhen et al, 1997/, rather it benefited much from the three major investigations pertaining to the Äspö area, which were conducted during 2000-2002, see /Staub et al., 2002, Röshoff and Lanaro, 2002 and Hakami et al., 2002/.

4 Evaluation of primary data

4.1 Data from In-situ stress measurements

Over more than a decade stress measurements have been performed in boreholes sunk at a number of places in Äspö area. Different measurement techniques have been employed and in general - because of the different techniques used - no good correlation may be found among the measurement results. Table 4-1 includes some information on the method used and data sources for 6 boreholes; some of which were located in the vicinity of the HQ3 area. HQ3 area is located in the north side of the F-tunnel; a map of the area appears in /Hansen and Hermansson, 2002/. Measurements from 45 points in boreholes were collected. Data points were situated within the depth interval 330 - 550 m.

Table 4-1. Boreholes from which results from stress measurement were collected.

Borehole	Method	Data Source	Reference
KA2599G01	HF	SICADA	Klee and Rummel (2002)
KF0093A01	HF	SICADA	Klee and Rummel (2002)
KAS02	HF	SICADA	Bjarnarson et al. (1989)
KF0093A01	OC (Borre Probe)	#???	
KAS05	OC (Borre Probe)	SICADA	Bjarnarson et al. (1989)
KK0045G01	OC (Borre Probe)	IPR-02-03 #(not printed)	Klasson et al. (2002)
KA2510	OC (CSIRO)	# PR-25-94-02[1)]	# Stille et al (1993)

1) Reference cited in report /Beatrice Lundholm, IPR-00-24, 2001/.

HF denotes the Hydraulic Fracturing technique and OC denotes the Overcoring method. Results from measurements performed by Deep Door Stopper Gauge System (DDGS) were not taken into consideration as it was found that systematic deviations existed when compared with results from either HF or OC methods.

The overcoring method Bore Probe and the Hydraulic Fracturing technique measure the magnitude for the minor principal stress. The magnitude of the major principal stress, σ_1, is not measured directly; it is derived through a mathematical expression, see for example /Amadei and StepHansen, 1997/. Table 4-2 shows ranges for σ_3 magnitudes obtained from the measurements.

Table 4-2. The magnitudes of the minor principal stress σ3 from the in-situ measurements.

Number of data points	Range for σ_3, MPa
36	5-19
28	6-12

The magnitudes of the major principal stress, σ_1, measured directly or derived from the different techniques mentioned vary considerably. Table 4-3 shows the ranges for the major principal stress σ_1 obtained from the overcoring method and the Hydraulic Fracturing technique.

Table 4-3. The magnitudes of major principal stress σ1 from the in-situ measurements.

Measurement technique	Range for σ_1, MPa
Overcoring	18-36
Hydraulic fracturing	18.7-26.3

Table 4-4 shows the values for the intermediate principal stress, $\sigma_{2\ that}$ were obtained by the overcoring method.

Table 4-4. The magnitudes of the intermediate principal stress σ2 from the overcoring measurements.

Number of measurements	Range for σ_2, MPa
4	10-22
14	14-18

It should be noted that the variation in values also depends on the depth range of 330-550 meter, where the measurements had been taken. As a quick comparison, the values given for σ_2 given in Table 5-4 may be compared with the magnitudes of σ_v induced by the weight of the overburden rock, i.e.

$\sigma_v = \zeta\ g\ h$

In which ζ is the rock density,

g is the gravitation acceleration and

h is the depth.

The approximate magnitudes of the vertical stress, σ_v, for the depth range mentioned, is 9-15 MPa.

4.1.1 Stress anisotropy

It is very informative to consider the ratio between the major principal stress and the minor principal stress, as it simply indicates the stress anisotropy that is found within the area in question. Results from 14 measurements performed by overcoring technique in borehole KF0093A01, KK0045G01 and KA2510A yield the σ_1/σ_3 ratio to be in the range of 2.1 –4.8, with an average value being equal to 3.4. As regards the measurements taken by Hydraulic Fracturing technique, the average ratio, where 6 measurement points in the vertical borehole KA2599G01 had been checked, was 2.0. For the borehole KAS02, where 8 measurement points in the range of 350 – 550 m were taken into consideration, the ratio was 1.8. The HF ratio is closely comparable with the lower limit of the range for the ratio calculated from OC measurements.

4.1.2 Initial state of in-situ stress

Based on the in-situ stress measurements performed at Äspö, an initial state of stress had earlier been evaluated /Hakami et al 2002/, in which the variation of the major, the intermediate and the minor principal stress with depth was obtained by a linear regression analysis performed on the data available. Figure 4-1 shows the variation of the principal stresses obtained.

The state of stress as described above may be referred to as the initial state of stress, where the influence from the existing major structures is absent and it does not reflect the inhomogeneity in the stress field as caused by those structures. In other words, the state of stress as such may just be valid within the very limited volumes of rock that are adequately far from the geological structures.

The equations that describe the variation of the principal stresses, σ_1, σ_2, and σ_3 with depth are:

$$\sigma_1 = 0.065\ Z + 1 \quad \text{MPa}$$

$$\sigma_2 = 0.027\ Z \quad \text{MPa}$$

$$\sigma_3 = 0.0174\ Z + 3.3 \quad \text{MPa}$$

The equations given above were derived from the final model analysis carried out within the framework of Test Case project /Hakami et al., 2002/.

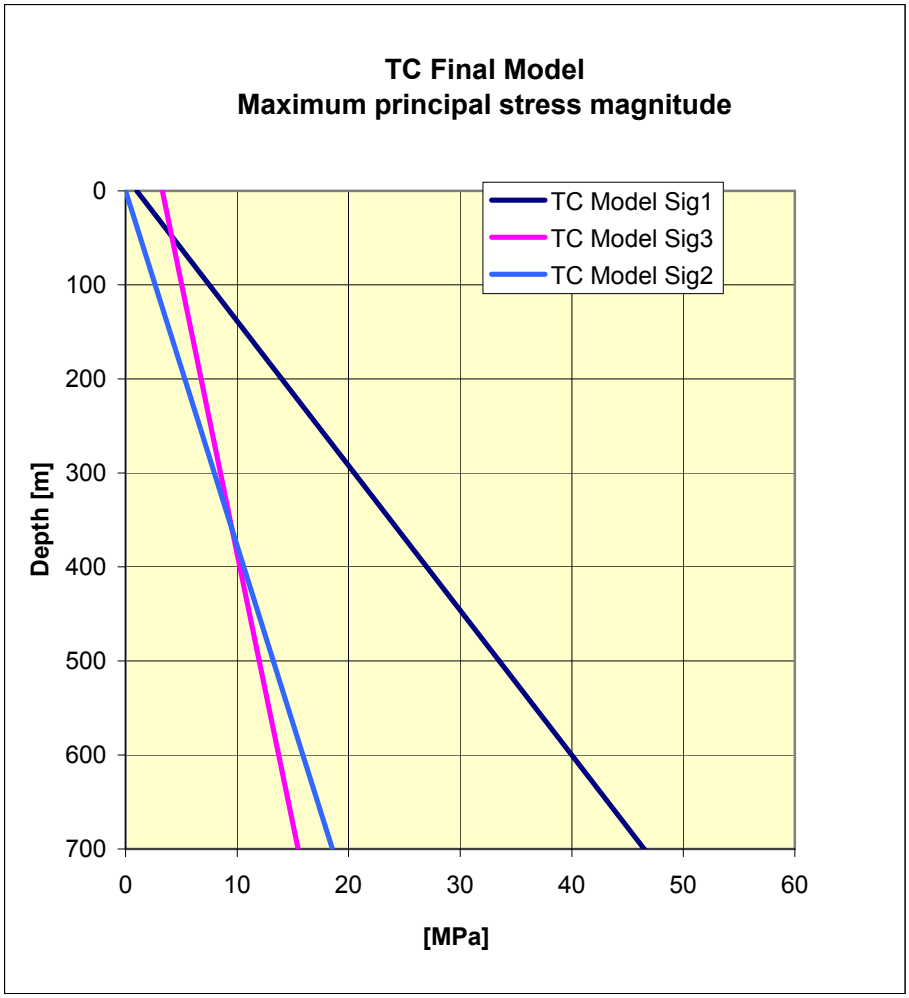

Figure 4-1. *The variation of the principal stress distribution versus depth derived from the final 3DEC model analysis /Hakami et al 2002/.*

4.1.3 Orientation of the in-situ stresses

From the measurement results, data were collected on the trend and the plunge of the principal stresses. The measurements from the OC technique, taken inside the horizontal borehole KF0093A01, show clearly that the orientation of the principal stresses is not parallel with orthogonal axes lying in horizontal/ vertical planes. The major principal stress σ_1 plunges towards NW with a bearing of 295°-298°. The two measurements in the borehole taken at about 3 and 5 meters from fracture J1 (Figure 5-3) yield values of 38° and 10° for the plunge of σ_1 respectively.

All data collected show that the trend of the major principal stress lies in the range of 106° –160° from the magnetic North. Out of 31 values checked, 22 were in the range of 115°-145°.

The plunge of the intermediate principal stress was also extracted from the measurement results, which falls into the range of 30°- 80°.

4.2 Mechanical properties of rock mass

In rock mechanics literature, a rock mass is commonly defined as a volume of rock that contains fractures of almost any size. The assumingly intact parts of the rock mass; which, nonetheless, contain large quantities of micro and even small fractures, are called rock matrix. Accordingly, rock mass may be then divided into rock matrix and fractures; fractures that are larger than –as a tentative value – few centimetres.

In comparison with the most commonly used terminologies given above, exceptions are made in the rock mechanics part of this report. By rock mass it is meant that it excludes all large fracture zones and even well defined single fractures, which enter the 3DEC modelling as independent entities. Rock matrix, as defined in the first paragraph, does not enter the numerical analyses. As a result we may hereafter refer to rock mass, distinct fractures and fracture zones ((even other structures such as fracture swarms) instead of referring to rock matrix and fractures.

During years 1999-2002 comprehensive studies were carried out, in which the rock masses existing at Äspö area were characterized in greater details, in order to establish their mechanical properties. The nature of the investigations were both empirical, see /Röshoff, Lanaro and Lanru, 2002/ as well as numerical (theoretical), see /Staub, Fredriksson and Outters, 2002/. Shortened versions of the works mentioned appeared in /Andersson, Christiansson and Hudson, 2002/.

As it was judged unlikely that the mechanical properties of the rock mass limited by GeoMod boundaries differ noticeably from those derived for the rock masses found within the so called Test Case area (see the references above), it was decided that the mechanical properties, needed for the numerical modelling reported here, be extracted from the works referred to in the previous paragraph.

From a comparison of the intervals presented for the modulus of deformation, it was decided that a value of 40 GPa should be appropriate to use as the input data representing the rock mass in the in the 3DEC analyses.

4.3 Mechanical properties of the fracture zones

Mechanical properties of a number of fracture zones found in Äspö area were studied by /Röshoff et al, 2002/, to the extent that the available borehole data entries in SICADA would allow. As band-like rock masses with higher intensity of fracturing and likelihood of high degree of alteration within the core part, fracture zones were characterized in the same way as neighbouring rock masses. No distinction was made in ways of deriving the modulus of deformation for the fracture zones, rather they were treated as other rock masses, found within the investigation limits. The modulus of deformation derived for rock parties that were contained within the limits of the fracture zones were not reported separately, rather they were included in tables, which listed the deformation moduli from all rock parties studied.

In 3DEC analyses, fracture zones were incorporated into the modelled rock block as planar structures with no thickness. To include the effect of the presumably highly fractured band-like rock mass belonging to a fracture zone, both the normal stiffness and the shear stiffness assigned to the planar structure were calibrated against the thickness of the fracture zone. In this way a fracture zone with, for example, a thickness of 5 m entered the computations as a stiffer inclusion compared with where the fracture zone had a thickness of, e.g. 20 meters.

Friction angle, an important parameter that controls the shearing of a fracture, is a well known-and studied parameter as long as it concerns single, well-defined fractures. The overall frictional property of facture zones, however, is much less studied. Yet the data available for this parameter, which mainly are found in earthquake research, see for example /Li, 1986/ and structure geological investigations are sufficient to resort to for our purpose. In general the overall friction angle that may be related to a fracture zone is considered to be lower that the friction angle for a well defined single fracture. The values for the friction angle of the structures that were modelled in the 3DEC analyses will later be given in the relevant sections.

5 Tree-dimensional site descriptive modelling

5.1 3DEC program

The program 3DEC (Itasca 1998) used to perform the numerical analyses in this work, is based on the distinct element method. This methods falls within the general classification of discontinuum analysis techniques. A discontinuous medium is distinguished from a continuous medium by existence of interfaces or contacts between the discrete bodies that comprise the system.

The main features of the program may be summarized as:

- Simulation of large displacements (slip and opening) along distinct surfaces in three-dimensional discontinuous medium; e.g, jointed rock masses.
- Discontinuous medium treated as an assemblage of discrete (convex or concave) polyhedra; concave polyhedra created by joining together convex polyhedra.
- Discontinuities are treated as boundary conditions between blocks.
- Relative motion along discontinuities governed by linear and non-linear force-displacement relations for movements in both the normal and shear directions.
- Explicit solution scheme, giving stable solution to unstable physical processes.
- Blocks may be rigid or deformable.
- Two types of material models for deformable blocks, elastic or Mohr-Coulomb plasticity.
- Two types of material models for discontinuities; Coulomb slip or continuously yielding.

5.2 General modelling assumptions

Any numerical analysis indeed involves a number of assumptions and simplifications. To give an example, it is very common that the possible variation in the modulus of deformation that is encountered when a cross over is made from a rock party to the next is neglected and the existing rock masses are treated identically. Or when the rock fractures are modelled, their irregularities are normally not taken into consideration and they are instead modelled as planar structures.

In the current work, the rock mass was modelled to behave as an elasto-plastic material. Only one value of rock deformation modulus was taken into consideration, representing all rock masses contained in the numerical modelling.

Regional and major fracture zones were important entities that were incorporated in the modelling work. They were modelled as planar structures despite the fact that they are indeed very irregular in shape. The behaviour of these structures was chosen to be described by the coulomb slip /Itasca, 1998/.

In order to take account of the thickness of the fracture zones, the values of the normal and shear stiffness of fracture zones was calibrated against the thickness of each fracture zones as determined by structure geological investigations conducted at the site.

When setting up the geometrical model of an area of interest for the purpose of numerical analysis, based on which a grid for numerical computations is constructed, it is important to select the outer boundaries, normally the side walls of a right-angled parallelepiped, at large distances from the target area such that any mechanical influence from those boundaries on the target area be cancelled. Yet the boundaries cannot be selected too far, as the computation grid would then turn to contain a large number of computational cells and this either may not be handled by the personal computers used or the computational time becomes impractically long.

In order to set the boundaries at optimal distances from the target areas pertaining to this study, a number of computations were made on rock blocks in which the boundaries had different distances from the target area. The most optimally located boundaries were then chosen, on which the mechanical boundary conditions were imposed.

The mechanical boundary conditions that were used for all analyses carried out in this work were:

a) The so-called “no displacement boundaries”, which means that the boundaries in question are not allowed to undergo any displacements perpendicular to the plane of those boundaries. This condition was imposed on all the sidewalls of the modelled block and on its bottom side.

b) No boundary condition was imposed on the topside of the modelled rock block. This condition allows for any inside deformations and /or displacements to expand to the surface facing no hinder

5.3 HQ3 area

5.3.1 Foreword

In pursuing the plans for enhancing the in-situ stress measurements within Äspö, SKB had chosen to sink two new bore holes within HQ3 area (see /Hansen and Hermansson, 2002/), in which a number of stress measurements were performed. Structure geological investigations that were carried out in connection with the two bore holes and also investigations performed in a nearby tunnel (tunnel TASF, see Figure 5-3) together created a reserve of information that called for erecting a detailed structure geological model of the HQ3 area, see /Hansen and Hermansson, 2002/.

Having had the structure geological model of the HQ3-area available, it was decided that a numerical analysis should be performed over the area in order to see how and if minor fracture zones and /or well-defined and extended single fractures affect the stress field, which in general is highly influenced by major fracture zones.

Structure geological model of the HQ3 area

The structure geological model of the HQ3 area is detailed in /Hansen and Hermansson, 2002/. The model covers two target areas, a cube with a side length of 200 m and a smaller one with a side length of 50 meters. The coordinates of the two blocks are given in Table 5-1.

Table 5-1. Target rock blocks within the HQ3 area.

Model block	Origin E	Origin N	Origin Z	Width dx	Length dy	Dz	y-axis bearing
200m	1551213.0	6367730.0	-350	200	200	-200	348.2
50m	1551295.0	6367804.5	-430	50	45	-45	346.0

The location of the 200-m cube in relation to the major fracture zones EW1a, EW1b, EW3, NE1 and NE2 crossing the Äspö area is shown in Figure 5-1.

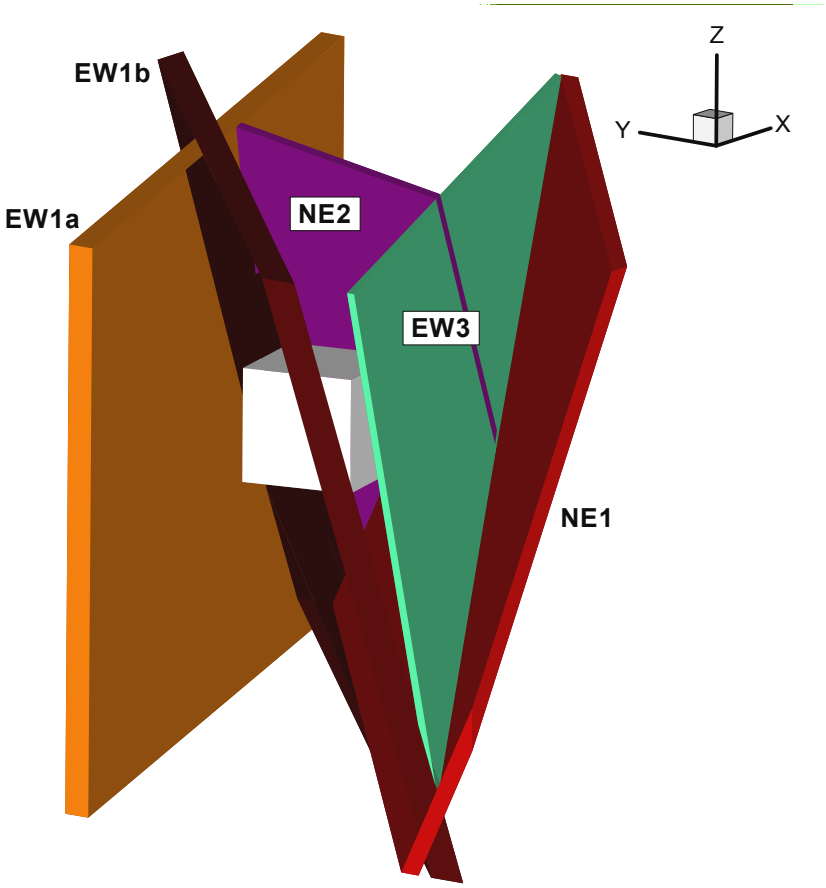

Figure 5-1. *The location of the target area with side length of 200 m, in relation to the major structures.*

The local structures that are found within the HQ3 area are listed in Table 5-2 together with sources for information given and geological descriptions.

Table 5-2. Local structures in the HQ3 area after /Hansen and Hermansson, 2002/.

ID	Mapped occurrences in Tunnels (TA...) or borehole (K...)	ID or description, width, minerals	Orientation	Data source
NE-HQ3	TASA ch 3520	Fracture Zone Z4	NE sub-vert.	PR 259528
	TASF- TASJ junction	Fracture Zone	NE sub-vert.	PR 259528
	TASA ch 2740	Fracture zone Z2	NE steep SE	PR 259419
	KAS 13	RQD< 25	No data	SICADA
	KA3010, 22.87 – 25.00 m	Mylonite	No data	SICADA
	KA2598A, 70-76 m	RQD<25, incr fract, breccia(106) & tect (108)	No data	SICADA
	KF 0093A01	Foliation at end of hole	No data	SICADA
	KJ 0044F01	Mylonite and increased fracturing at end of hole	No data	SICADA
NW-hyd	TASF ch 60-70	Zone w 4 parallel water bearing fractures	NW sub-vert	PR 259528
J2	KF 0093A01, 16.25m,323/80 KA 2599G01, 90.14m, 325/76	Granodiorite, 1-2mm, r, ep cl ca	NNW/steep East	SICADA
J1	KF 0093A01, 29.28m,355/47	Granodiorite,1mm,cl	N/moderate east	SICADA
H1	KA 2599G01, 111.99m	Granodiorite, 1mm, r, cl	93/17	SICADA
H2	KA 2599G01, 120.64m	Granodiorite, 1mm, r, cl	55/7	SICADA
H2	KA 2599G01, 120.64m	Granodiorite, 1mm, r, cl ca	23/2	SICADA
Abbreviations: r=rough, s=smooth, ep=epidote, ca=calcite, cl=chlorite				

Figure 5-2 shows a horizontal section through the 50m-cube target area at –455 m depths. The traces of some of the structures listed in Table 6.2 are shown on the section. The structures either terminate against each other or against the major fracture zones. Among the structures, the fracture zone NE-HQ3 striking NE is the most dominant one.

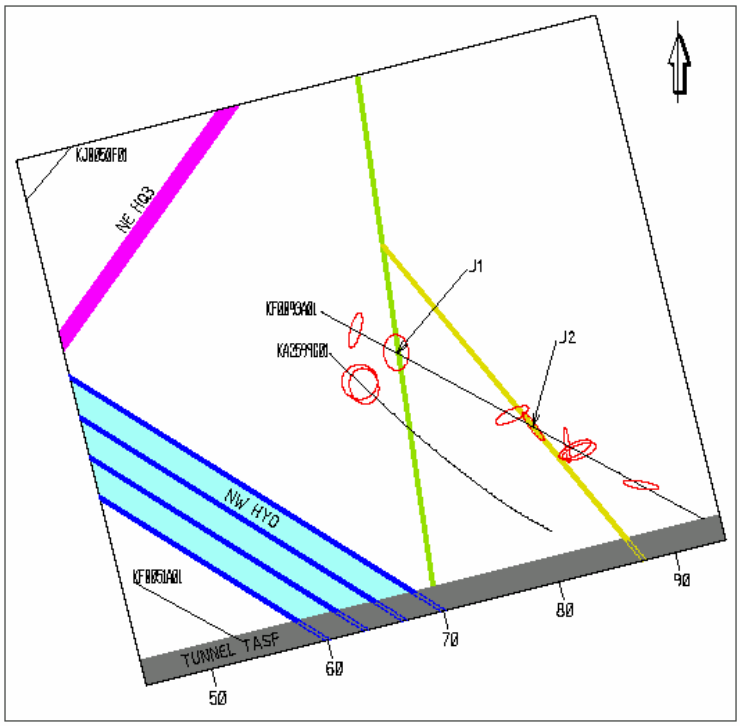

Figure 5-2. *Horizontal cross-section at –455 m depth through the 50 m target area within the HQ3 area, after /Hansen and Hermansson, 2002/.*

Fracture swarm NW-HYD, being also sub-vertical and striking NW was modelled as four single fractures. The four fractures terminate at NE-HQ3.

The sub-vertical borehole KA2599G01 and the sub-horizontal borehole KF0093A01 are shown in Figures 5-2 and 5-3. Figure 5-3 is a vertical cross section through the 50m cube, viewed from South West.

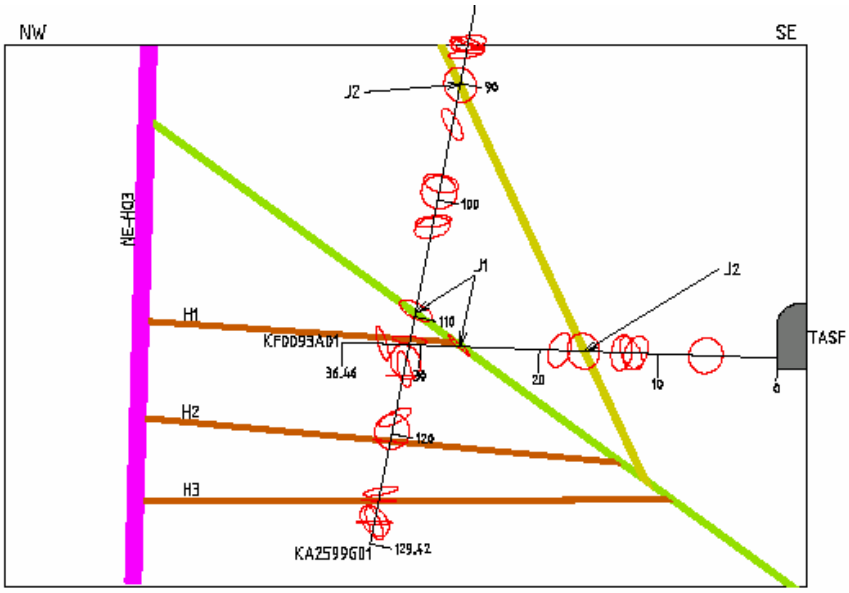

Figure 5-3. *Vertical cross-section of the 50 m box in the HQ3 area. Viewed from the SW, after /Hansen and Hermansson, 2002/.*

5.3.2 Numerical analyses

Having had sufficient data on the existing structures within the HQ3-area and the major fracture zones found in Äspö area, a large numerical grid was constructed, in order to eliminate any unwanted effects from the boundaries. A right-angled parallelepiped with an approximately 4.4 by 4.4 kilometres square cross section and a thickness of 4 kilometres was chosen to present the outermost boundaries of the grid. The sides of the right-angled prism were oriented parallel and perpendicular with respect to the orientation of the major principal stress. This way of orienting the grid facilitates the collection of data in sections that are parallel and perpendicular to the orientation of the major principal stress, σ_1.

A second volume of rock, here again a right-angled parallelepiped with a 3 by 3 square kilometres cross section and a thickness of 3 kilometres was set up in such a way to have parallel and perpendicular sides in relation to North. This second volume of rock also defined the end points for the five regional major fracture zones that were incorporated in the grid. It was judged that the size of the fracture zones incorporated into the model in this way was optimal for the numerical computations planned.

The structures that are described in detail in /Hansen and Hermansson, 2002/ were incorporated into the model. This was done as the position in space for each fracture /fracture zone as well as its extent were known. If for a structure the extent was not defined then the structure was extended to terminate at a nearby-running major fracture zone. See Figures 5-4 and 5-5 showing a vertical and a horizontal section through the model block.

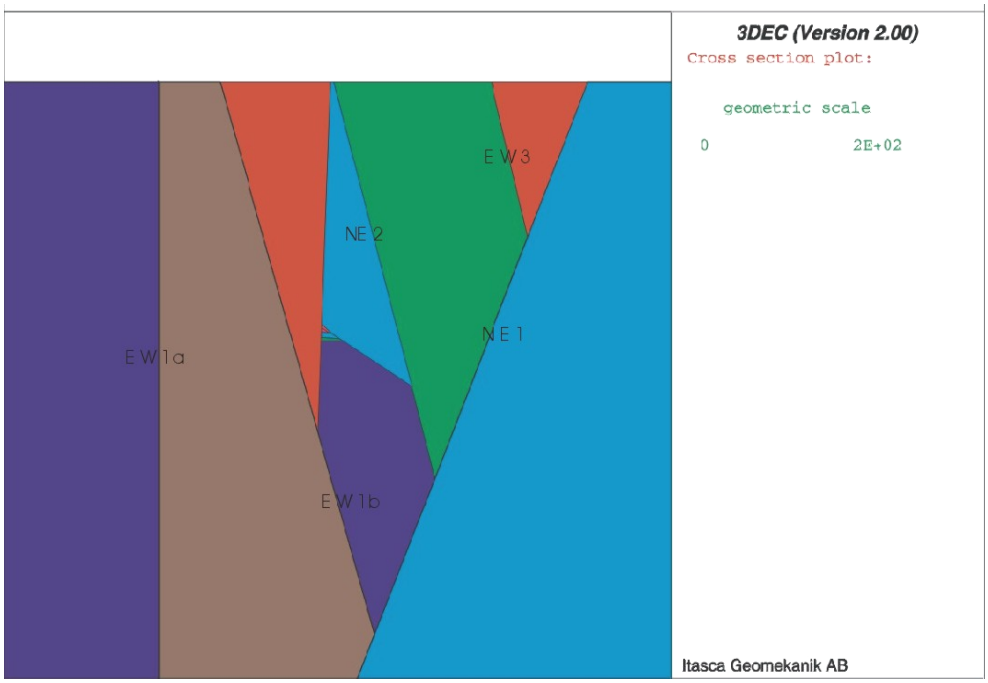

Figure 5-4. *Vertical cross section running parallel with NW-HYD (see Figure 5-2 for the location of NW-HYD). Note the scale of the local structures within HQ3-area compared with the scale of the major structures.*

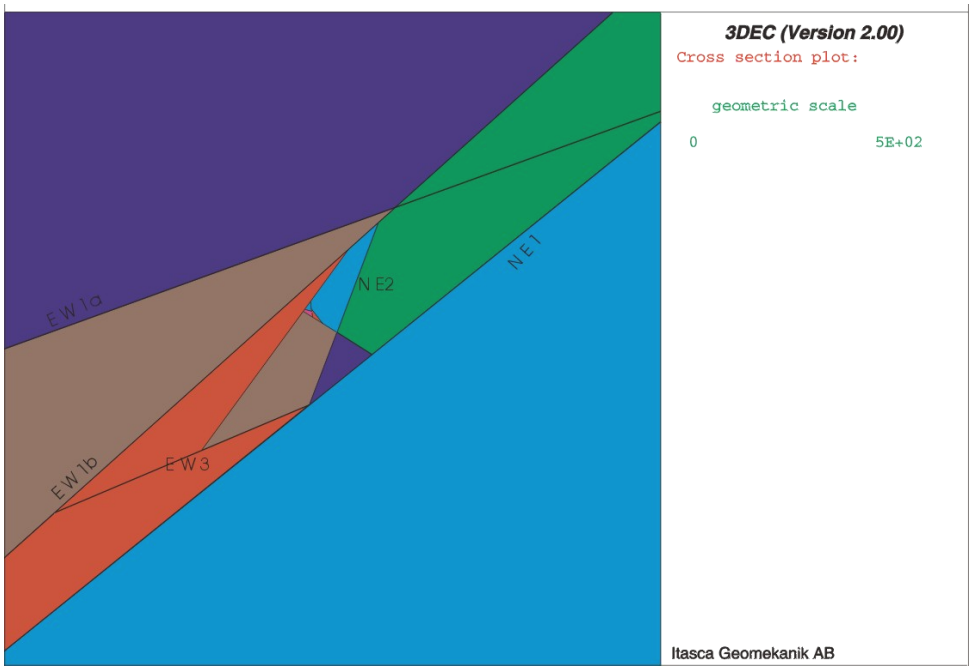

Figure 5-5. *Horizontal section taken at –455 m depth. Note the scale of the local structures within HQ3-area compared with the scale of the major structures.*

The coordinates of selected points used to position the fractures/fracture zones in the 3DEC model are given in Table 5-3. The estimates of the overall thickness of fractures/fracture zones are also added to the table.

Table 5-3. Data used to position the fractures/fracture zones in the 3DEC model.

Fracture/ fracture zone	Selected point			dip direction	dip	Width, meter
	E	N	Depth			
Major fracture zones						
EW1a	1551187.794	6368054.774	0	180	90	45
EW1b	1551220.754	6368014.867	0	138	75	50
NE2	1551356.698	6367801.843	-193.415	157	75.80	25
EW3	1551294.692	6367576.200	0	110.73	79	14
NE1	1551477.8542	6367411.085	0	321	70	28
Minor fracture zones / fractures						
NE-HQ3	1551303.157	6367852.911	-430	305.68	88	1
NW-HYD	1551315.753	6367809.675	-430	31.98	87.23	10
J1	1551288.694	6367832.709	-431.266	81.54	41.43	0.01
J2	1551326.485	6367812.350	-430	52.7	69.2	0.01
H1	1551304.935	6367853.355	-448.061	195.41	17.60	0.01
H2	1551319.575	6367857.005	-461.254	147.00	6.00	0.01
H3	1551327.102	6367858.881	-468.036	90.00	0.0	0.01

A very dense discretization was used within the HQ3-target area in order to increase the geometrical closeness of the points, from which desired data were to be collected, see Figure 5-6. The tetrahedrons forming the discretization zones in that area could not have any length exceeding 20 meters.

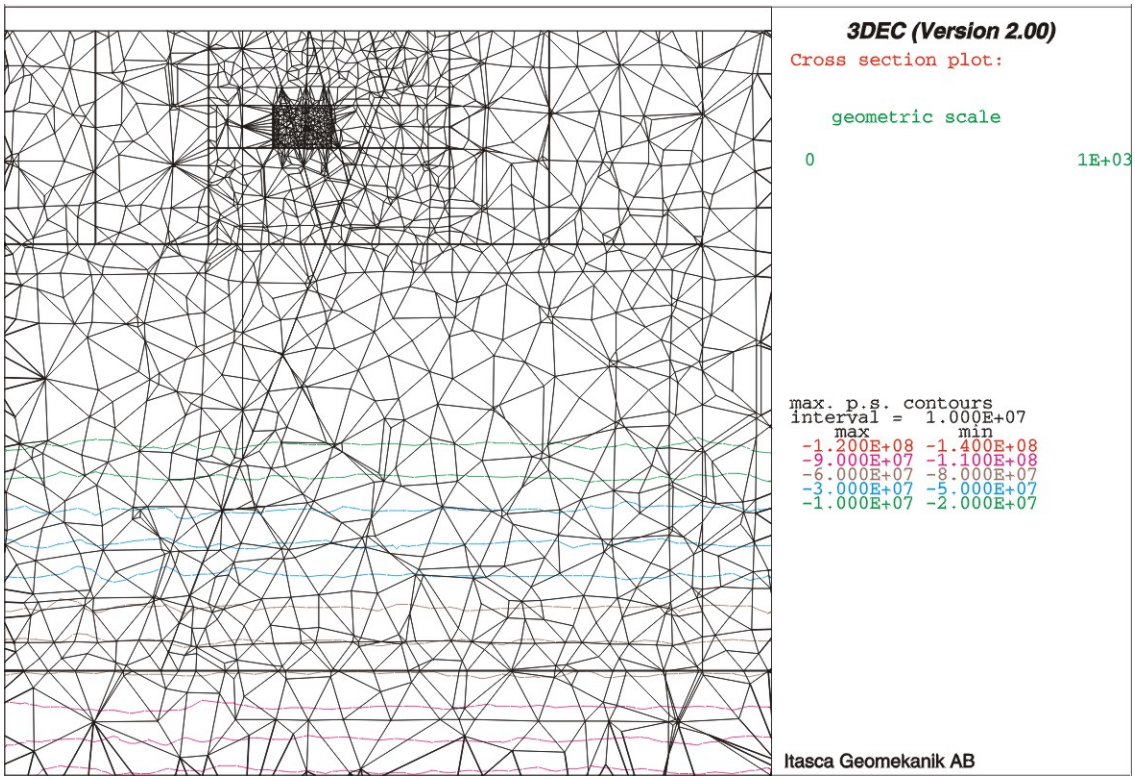

Figure 5-6. *Vertical section, showing the discretization of the Model. Discretization was much more dense inside the HQ3-area.*

5.3.3 Mechanical properties of rock mass and the fracture zones

/Lanaro and Röshoff, 2002/ carried out comprehensive investigations in order to assess the mechanical characteristics of the rock mass found in the Äspö area. Based on the classifications performed, the mechanical properties of the rock mass investigated were derived.

From the ranges specified for the modulus of deformation and the Poisson ratio, the typical values given in Table 5-4 were chosen as input parameters for the 3DEC model. The rock mass occurring in between the incorporated fractures/fracture zones was assigned the parameters given in table below.

Table 5-4. Mechanical properties of rock mass used in the 3DEC model.

	Modulus of Elasticity [GPa]	Poisson's ratio
Rock mass	40	0.25

It was assumed that all five regional fracture zones had identical mechanical properties, whereas varying mechanical properties were assigned to the fracture zones/fractures incorporated in the HQ3 area. The mechanical properties used for the structures incorporated are listed in Table 5-5.

All structures incorporated into the geometrical grid were formed as planar entities, without any physical thickness. The thickness estimates of the structures were, however, taken into consideration by reducing the stiffness of the planar structures proportional to their thickness. Both normal and shear stiffness of a structure were calibrated in this way. The water-bearing zone NW-HYD was assigned comparatively lower friction angle because of the abundance of water in that zone.

Table 5-5. Mechanical properties of the structures used in 3DEC analysis of the HQ3-area.

	Normal stiffness [GPa/m]	Shear stiffness [GPa/m]	Friction angle (°)
Regional fracture zones			
EW1a	0.01	0.005	15
EW1b	0.01	0.005	15
NE2	0.01	0.005	15
EW3	0.01	0.005	15
NE1	0.01	0.005	15
HQ3 area			
NE-HQ3	1.0	0.5	25
NW-HYD	1.0	0.5	15
J1	10	5	30
J2	10	5	30
H1	10	5	30
H2	10	5	30
H3	10	5	30

5.3.4 Displacements

Figure 5-7 shows the shear displacements that the fracture zones experienced when the 3DEC run was completed. The regional fracture zones underwent the largest shear displacements. The true length of the arrows indicates the different magnitudes of the shear displacement. Note, however, that the arrows are plotted in a perspective view and are not drawn to their true lengths.

It is clear from Figure 5-7 that only comparatively small and insignificant shear displacements were developed along the fracture zones found within the HQ3-area. Even though the fracture zone NE-HQ3 appears in the model with a relatively large size (the deeper end terminates against EW1b and the shallower end reaches the ground surface) it undergoes no significant shear displacement, simply because it dips almost at 90 degrees.

Figure 5-8 shows a horizontal section taken at the depth of -455 m.

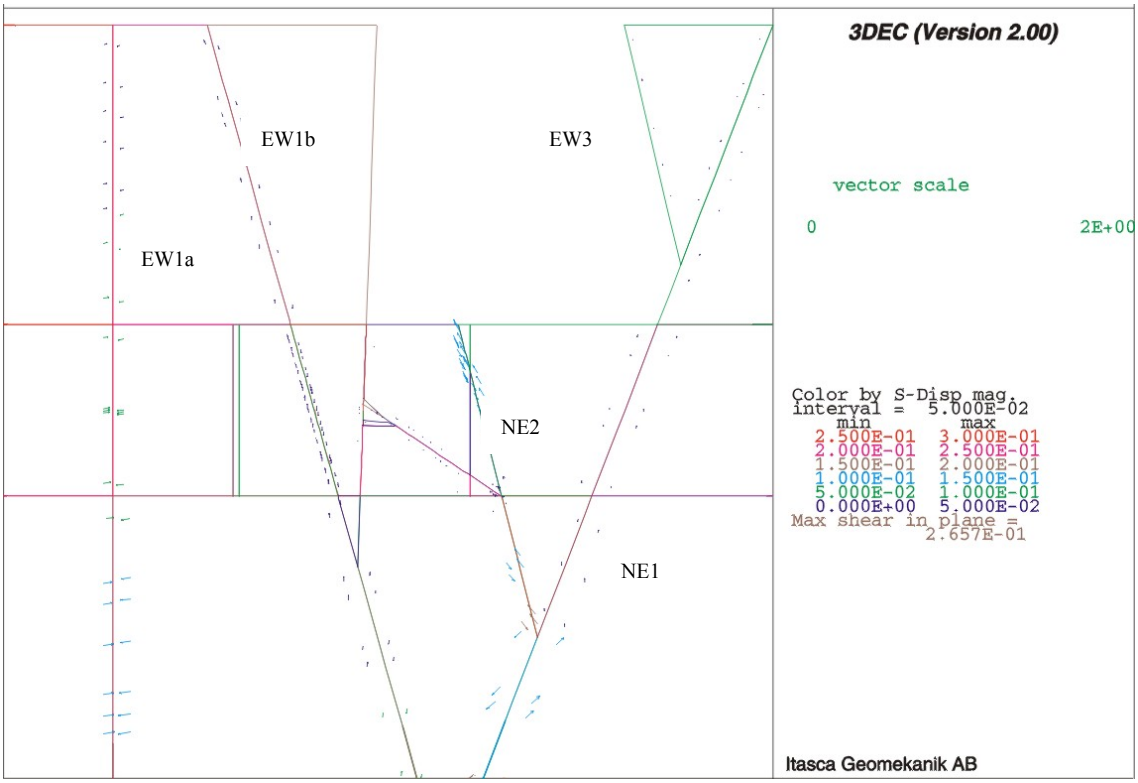

Figure 5-7. *Shear displacements along fracture zones. The vertical cross-section shown is parallel with NW-HYD. (see Figure 5-2 for the location of NW-HYD).*

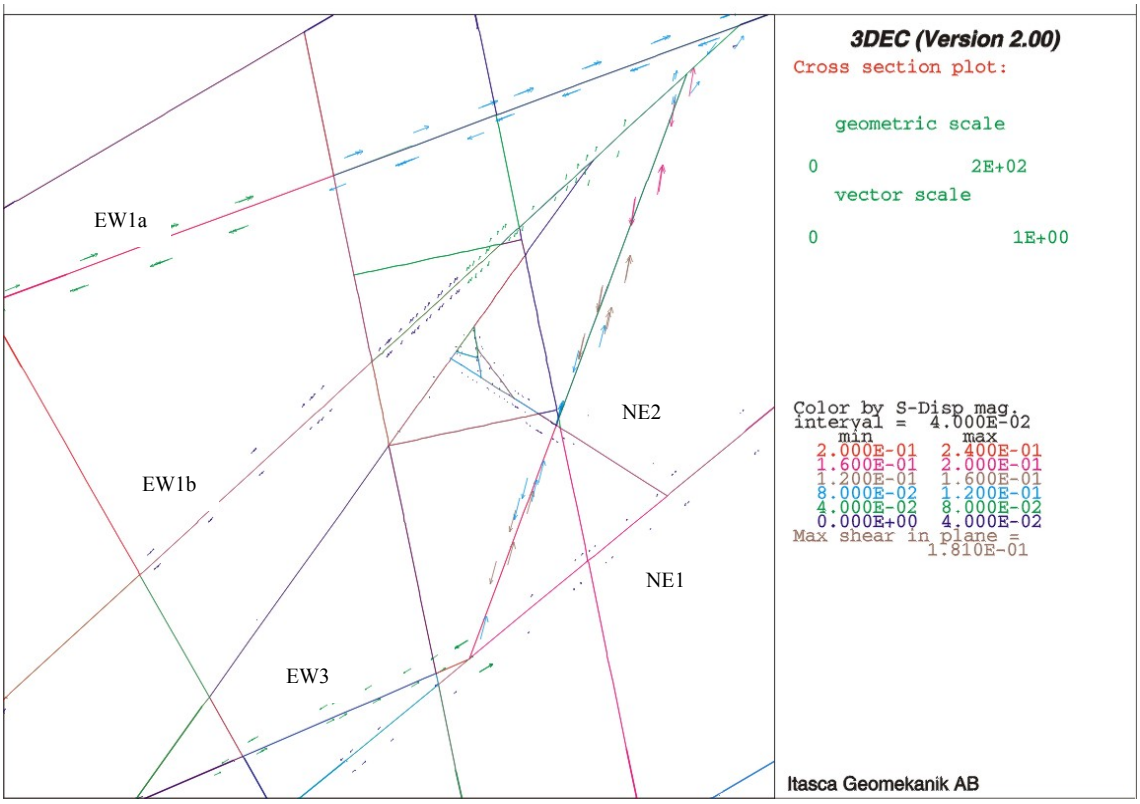

Figure 5-8*. Shear displacements along fracture zones on a horizontal section at –455 m depth.*

5.3.5 Stress distribution

In order to visualize the stress field, three orthogonal cross-sections through the 200-m target area were selected, See Figure 5-9. The two vertical cross-sections ran parallel and perpendicular to σ_1 respectively, passing through the centre of the block. The horizontal section was chosen at the depth of – 455 meters.

At times it may be more convenient to look at the vertical stress σ_V and horizontal stresses, σ_H and σ_h, instead of the principal stresses. σ_1, σ_2, and σ_3. Figure 5-10 shows the maximum horizontal stress σ_H and the vertical stress σ_V derived from the principal in-situ stresses. They are plotted on a vertical plane parallel to σ_1. On this figure and also on Figures 5-11 and Figure 5-12, the estimated width of the fracture zones were added in order to better visualize the scales involved.

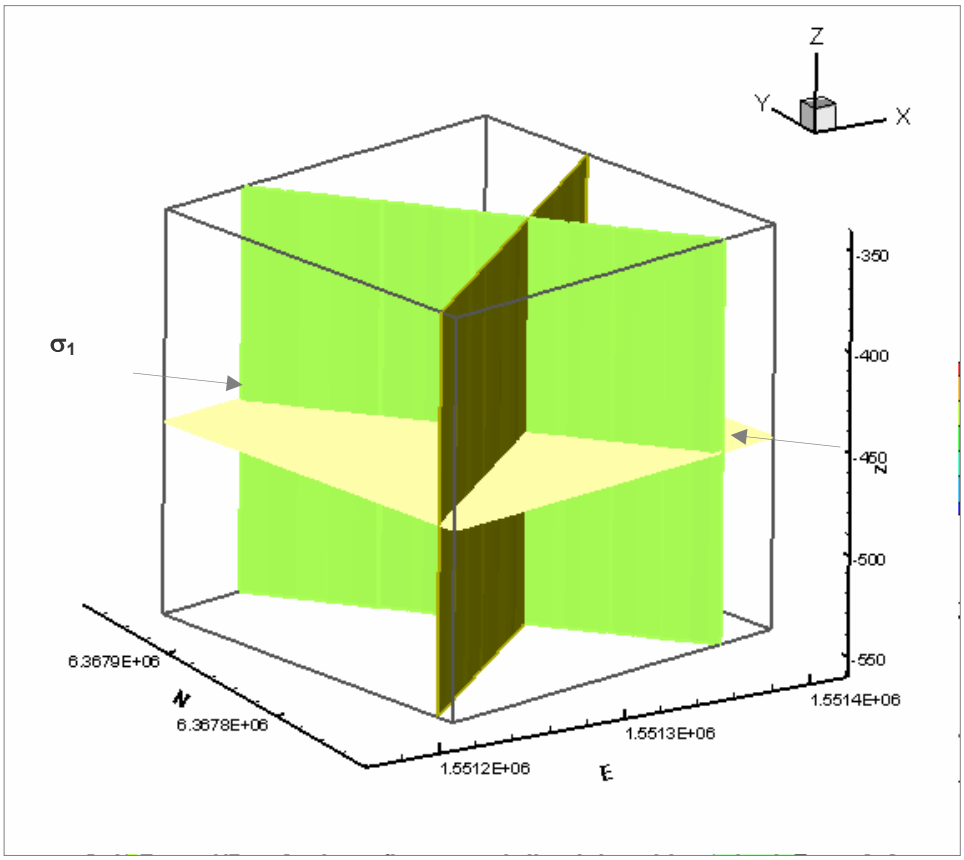

Figure 5-9. *The three orthogonal cross-sections on which the stress data were plotted. Note that the magnetic north is parallel with the y-axis and east parallel with the x-axis.*

Figure 5-10 shows the maximum horizontal stress, σ_H, and the vertical stress, σ_v, plotted on the vertical cross section that runs parallel to σ_1. In Figure 5-11, the minimum horizontal stress, σ_h, together with the vertical stress, σ_V is plotted on the cross section that runs perpendicular to σ_1. Figure 5-12 is the horizontal cross section at –455 m, on which the maximum horizontal stress σ_H and the minimum horizontal stress σ_h are plotted.

Figure 5-14 shows the position of the scanline. The magnitudes of the sampled principal stresses, their trends and plunges are plotted on Figures 5-14, 5-15 and 5-16.

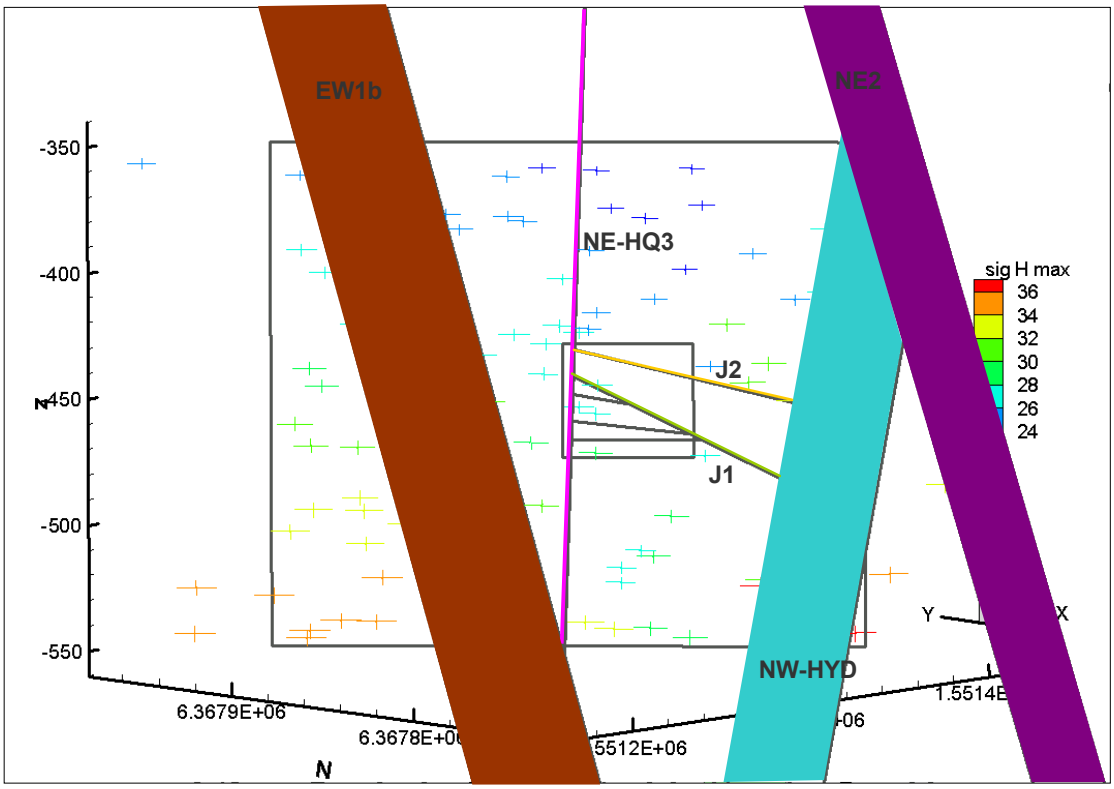

Figure 5-10. *Maximum horizontal stress (σ_H) and vertical stress (σ_v) in a vertical cross-section parallel to σ_1. Colour of the vectors refers to the magnitude of σ_H.*

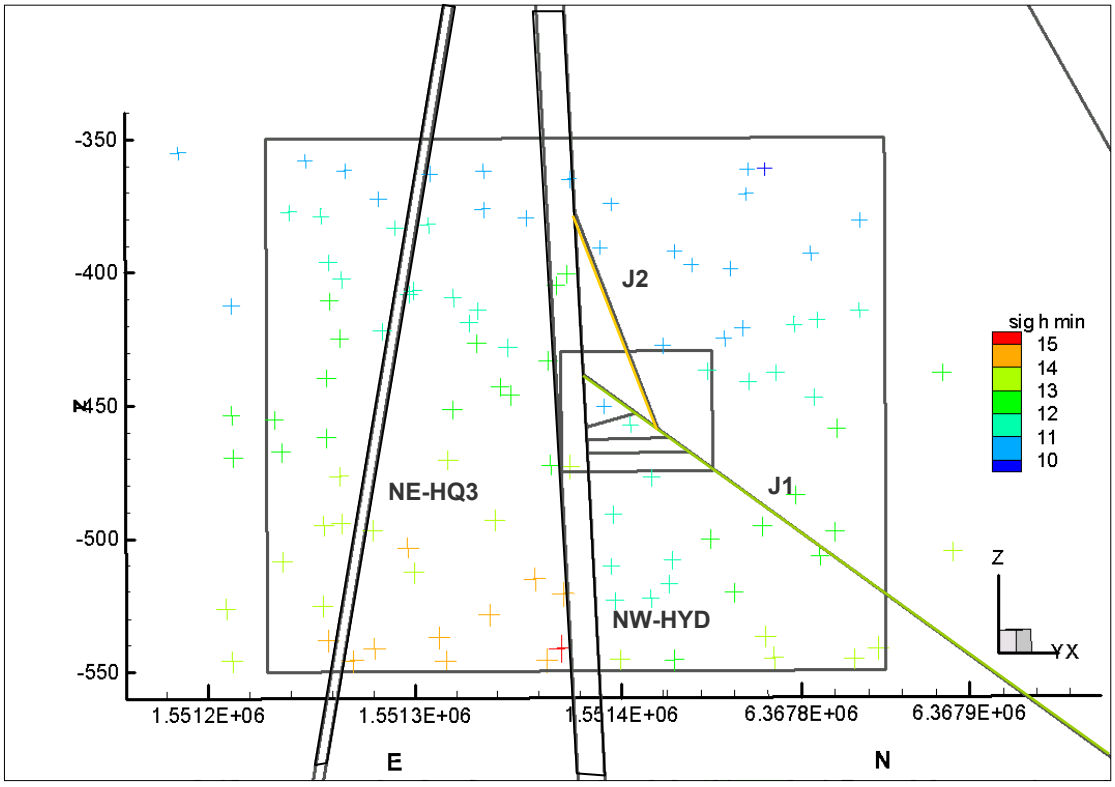

Figure 5-11. *Minimum horizontal stress (σ_h) and vertical stress (σ_v) in a vertical cross-section perpendicular to σ_1. Colour of the vectors refers to the magnitude of σ_h.*

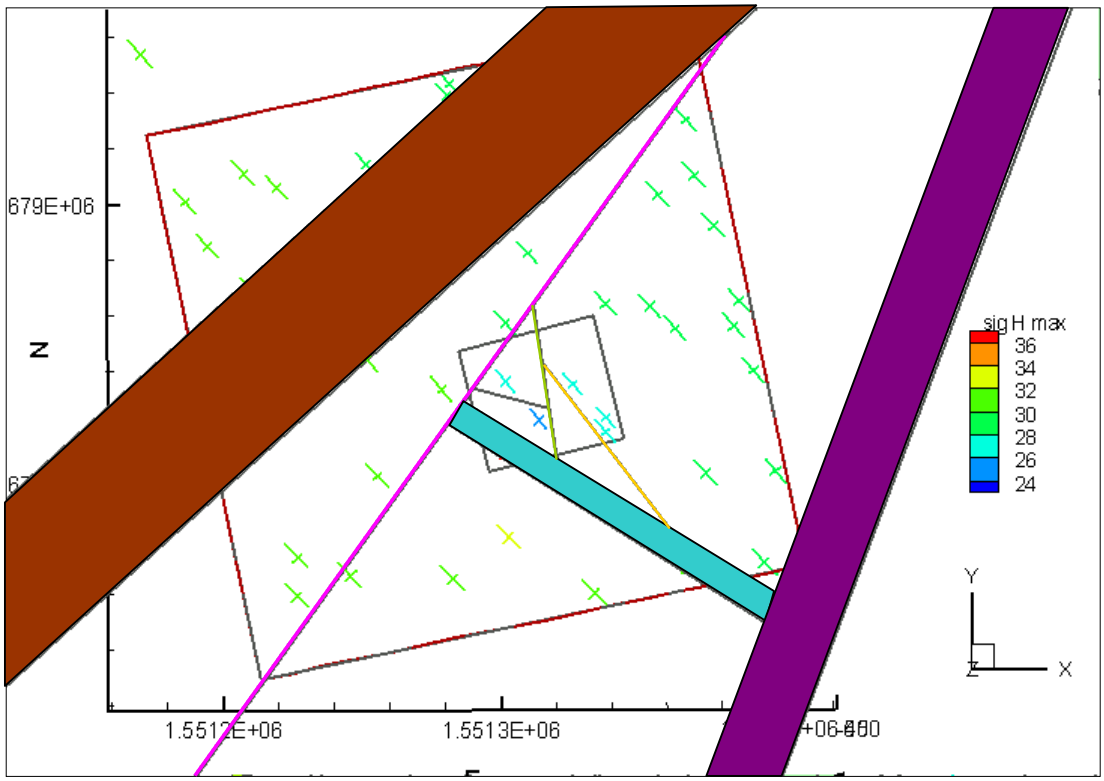

Figure 5-12. *Maximum (σ_H) and minimum (σ_h) horizontal stresses in a horizontal cross-section at -455 m depth. Colour of vectors refers to the magnitude of σ_H.*

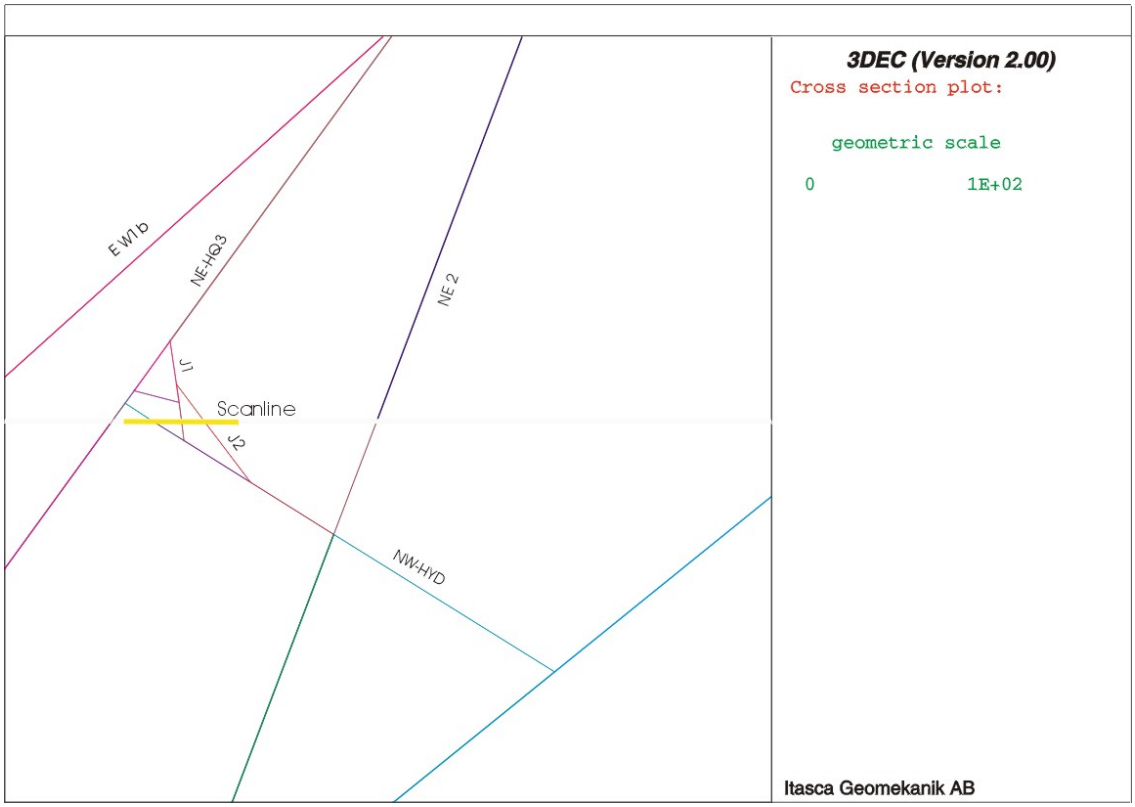

Figure 5-13. *The position of the scanline , along which principal stresses were sampleds. See figures 5.14, 5.15 and 5.16*

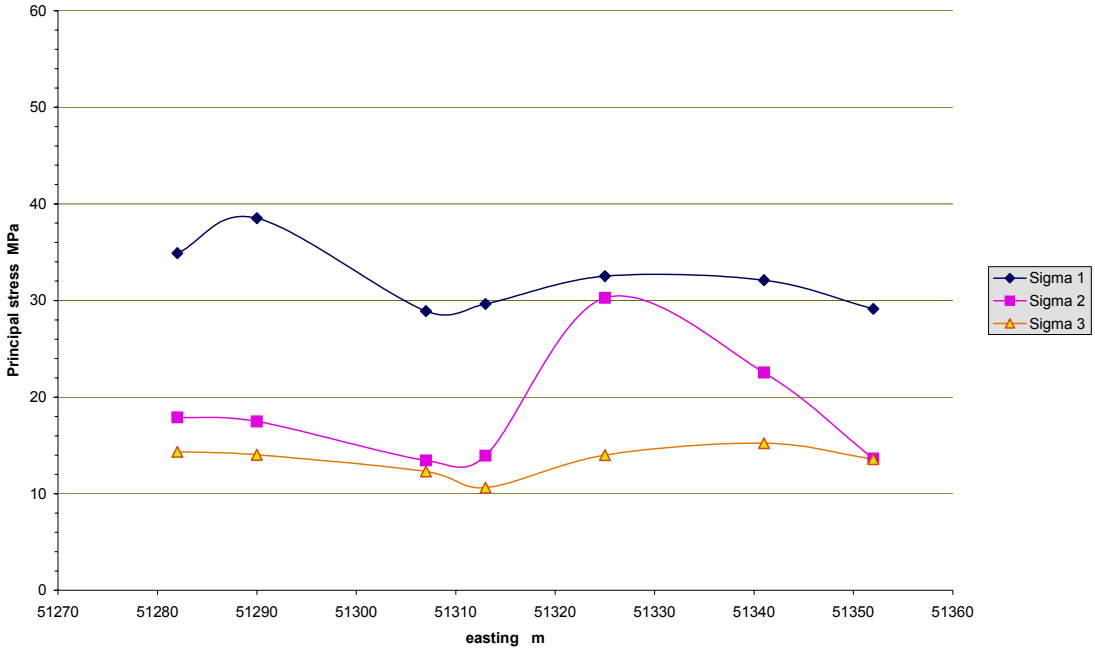

Figure 5-14. *The variation of principal stresses on horizontal level at –455 m depth.*

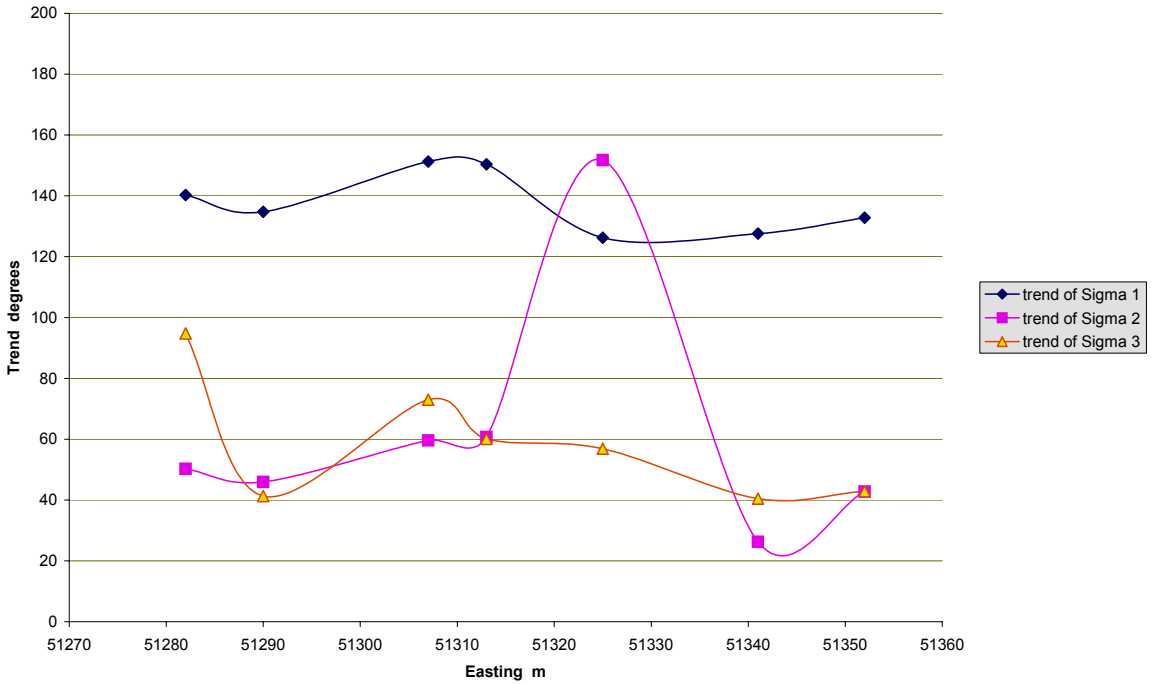

Figure 5-15. *The variation of the trend of the principal stresses on horizontal level at –455 m depth.*

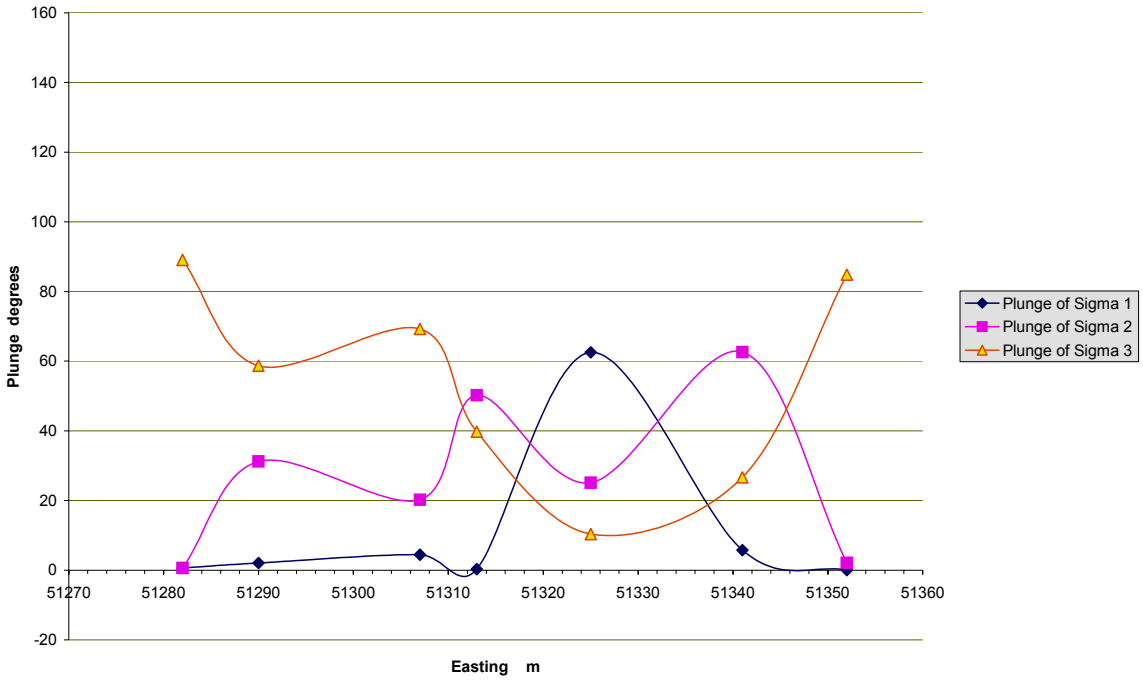

Figure 5-16. *The variation of the plunge of the principal stresses on horizontal level at –455 m depth.*

In order to make a comparison between the actual stress measurements and the stresses obtained from the 3DEC analysis, stress data from boreholes KA2599G01 (Hydraulic Fracturing) and KF0093A01 (HF, Over Coring) are plotted on Figure 5-17. Data on this figure includes:

- The computed magnitudes of the maximum horizontal stress, σ_H, and the minimum horizontal stress, σ_h, from the –455 m level.
- The magnitude of the minimum horizontal stress, σ_h, obtained directly from Hydraulic Fracturing performed in borehole KF0093A01.
- The calculated magnitudes of the maximum horizontal stress, σ_H, pertaining to Hydraulic Fracturing.
- The magnitudes of σ_H and σ_h from Over Coring measurements performed in borehole KA2599G01. The values were derived from the magnitudes of the principal stresses σ_1, σ_2, and σ_3 measured.

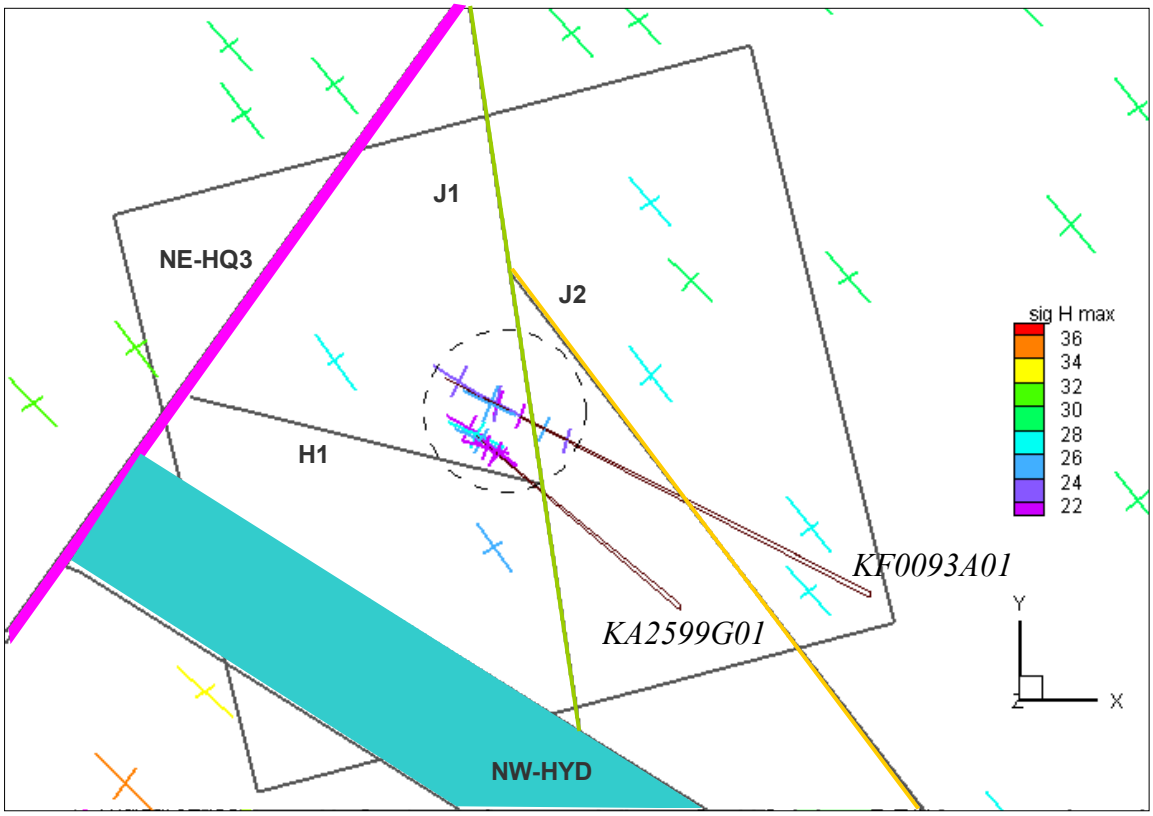

Figure 5-17. *The magnitudes and the orientations of σ_H and σ_h obtained from measurements in boreholes KF0093A01 and KA2599G01 (encircled), together with those derived from the 3DEC analysis, shown on a horizontal section. The cross bars representing σ_H and σ_h magnitudes are coloured by the magnitude of σ_H.*

5.4 GeoMod area

A 3DEC model block was set up that had a side length of 5345 m and a thickness of 4000 m. The model block contained two delimited rock volumes inside. The larger one, with a side length of 3000 m and a thickness of 3000 m, defined the size of the regional fracture zones. The smaller with a side length of 1000 m formed the GeoMod area, within which results from the numerical analyses were collected and illustrated. The corner coordinates of the GeoMod block are given in Table 2-1. In updating the structure geology of the Äspö site, the geology group, during the course of this project, chose nine major fracture zones to model. The nine fracture zones were incorporated into the 3DEC model, using the coordinates, the dip and the strike pertaining to each fracture zone as given in Table 5-6 and Table 5-7.

Table 5-6. The coordinates of selected points on fracture zones, extracted from The RVS model, used in setting up the 3DEC grid.

NE1_alt2		
x	y	z
1551194	6367109	50
1550923	6367579	-1000
1551701	6368232	-1000
1551972	6367762	50
1551194	6367109	50
1550923	6367579	-1000
1551701	6368232	-1000
1551972	6367762	50
EW1_b		
1550852	6367701	50
1550996	6367452	-1000
1551756	6368136	-1000
1551612	6368385	50
1550852	6367701	50
1550996	6367452	-1000
1551756	6368136	-1000
1551612	6368385	50
EW1_a		
1550742	6367893	50
1550742	6367893	-1000
1551696	6368240	-1000
1551696	6368240	50
1550742	6367893	50
1550742	6367893	-1000
1551696	6368240	-1000
1551696	6368240	50
EW3_alt3		
1551946	6367807	-51.585
1551933	6367830	50
1550970	6367498	50
1551044	6367370	-532.16
1551946	6367807	-51.558
1551933	6367830	50
1550970	6367498	50
1551044	6367370	-532.14

NE2		
x	y	z
1551536	6368181	-324.887
1551643	6368087	-854.438
1551295	6367491	-398.502
1551207	6367579	50
1551418	6368139	50
1551536	6368181	-324.959
1551644	6368087	-854.44
1551295	6367491	-398.49
1551207	6367579	50
1551418	6368139	50
HQ3_top		
1551054	6367408	-402.039
1551011	6367426	-276.818
1550944	6367543	50
1551288	6368094	50
1551470	6368117	-340.752
1551054	6367408	-402.001
1551011	6367426	-276.666
1550944	6367543	50
1551288	6368094	50
1551471	6368117	-340.711
HQ3_bottom		
1551028	6367547	-817.669
1551000	6367445	-700.666
1551033	6367389	-444.24
1551054	6367408	-402.075
1551470	6368117	-340.787
1551028	6367547	-817.666
1551000	6367445	-700.756
1551033	6367389	-444.193
1551054	6367408	-402.039
1551470	6368117	-340.753
NNW4		
1551487	6368115	50
1551611	6367914	-635.101
1551652	6367664	-208.427
1551611	6367719	50
1551611	6367914	-635.07
1551652	6367664	-208.418
1551611	6367719	50
1551487	6368115	50

NW1		
x	y	z
1551611	6367914	-634.289
1551540	6367945	50
1551362	6367990	50
1551550	6367928	-732.2
1551611	6367914	-634.253
1551540	6367945	50
1551362	6367990	50
1551550	6367928	-732.187
NW2		
1551922	6367849	-145.147
1551890	6367904	50
1551432	6368144	50
1551395	6368130	-115.175
1551478	6367942	-844.574
1551922	6367849	-145.102
1551890	6367904	50
1551432	6368144	50
1551395	6368130	-115.147
1551478	6367942	-844.573

Table 5-7. Fracture zones incorporated into the GeoMod model.

Fracture zone	Strike	Dip
NE1_alt2	230	63
EW1_b	48	75
EW1_a	70	90
EW3_alt3	71	76
HQ3_top	32	70
HQ3_bottom	209.516	77.705
NNW4	342.571	85.124
NW1	104.262	88.946
NW2	117.573	80.062
NE2	20.727	75.807

Figure 5-18 shows a perspective view of the 3DEC model block. The discretization may be seen on the block outer planes. In Figure 5-19, some of the prismatic portions constituting the outer block are removed in order to expose the inner block, defining the extent of the fracture zones.

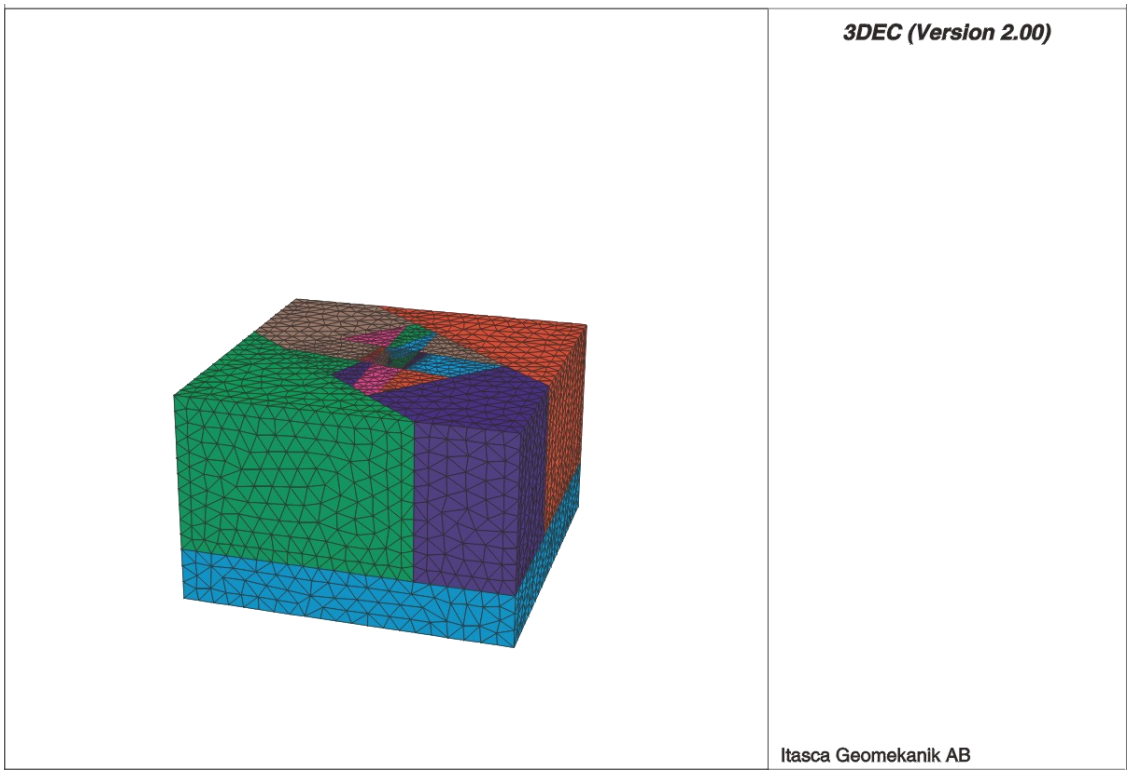

Figure 5-18. *Perspective view of the 3DEC model block. Discretization may be seen on the block outer planes.*

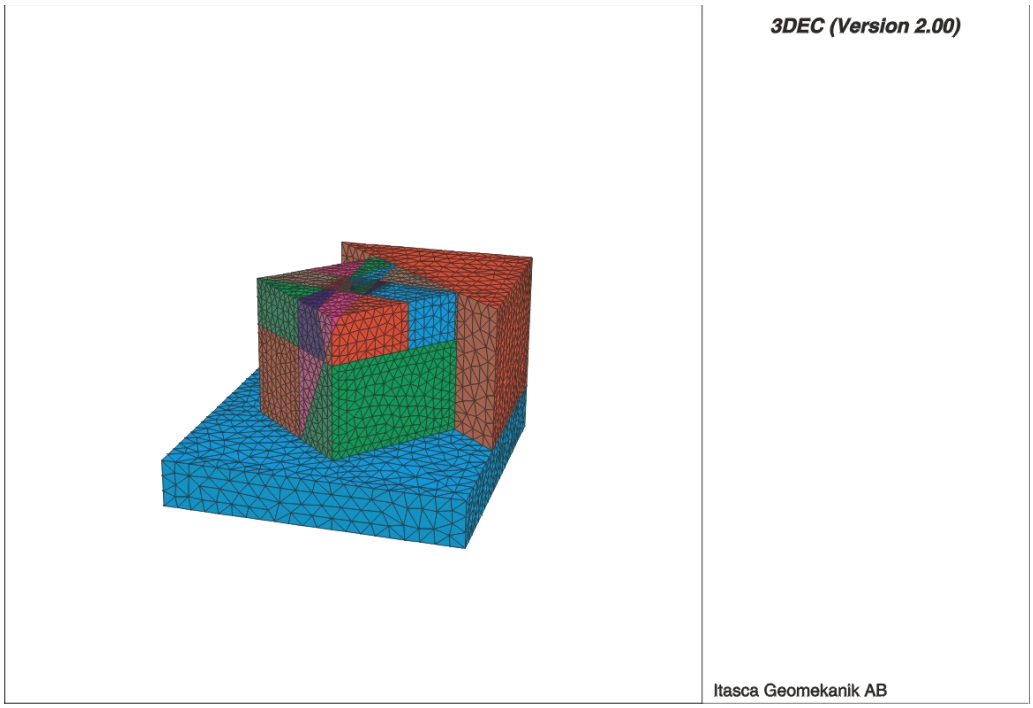

Figure 5-19. *Perspective view of the 3DEC model block, showing the inner delimited rock volume that defines the extent of the fracture zone incorporated.*

Figure 5-20 shows the nine major fracture zones as modelled in 3DEC. Zone HQ3, whose dip and strike change with depth was modelled as a folded surface as in the structure geological model.

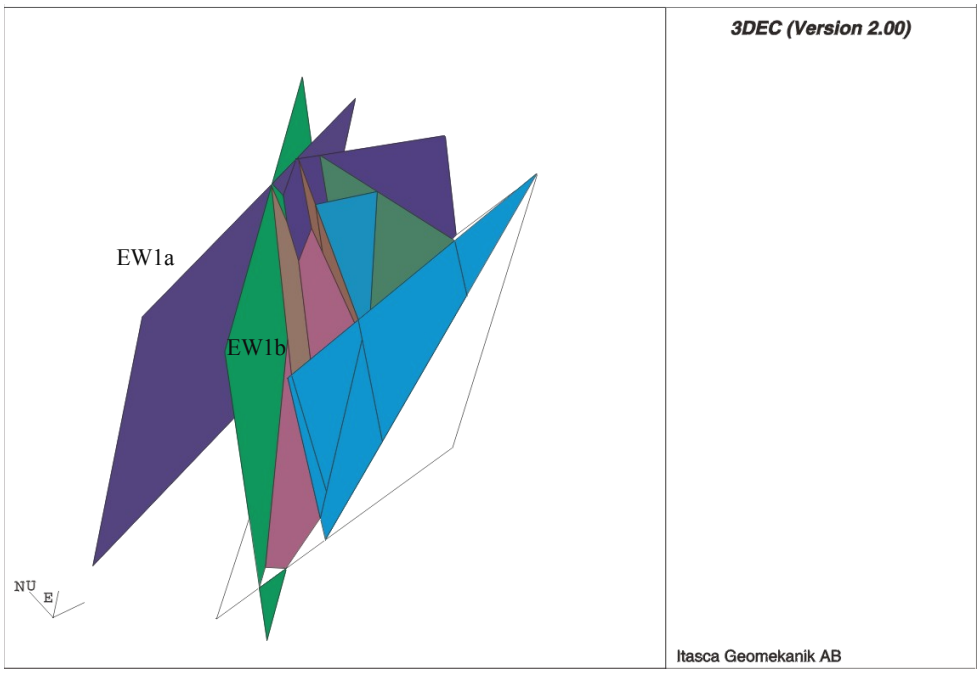

9 major farcture zones were incorported in the 3DEC-model

Figure 5-20. *The nine fracture zones as incorporated in the 3DEC model block.*

In order to assign balanced mechanical properties to the nine fracture zones incorporated into the 3DEC model, the fracture zones were tentatively divided into 3 categories, Table 5-8, following the available geological information.

Table 5-8. Categories tentatively defined to assign balanced mechanical properties to the fracture zones modelled.

Fracture zone name	Category
NE1, EW1B	Most extended
EW1a, EW3	Less extended
NE2, HQ3, NW2, NNW4, NW1	Least extended

The shearing behaviour of a fracture zone is controlled, among others, by the frictional properties of the surfaces in contact and how much stiff the fracture zone may be. When modelling, the approach adopted in defining the shearing behaviour of fracture zones modelled was based on the notion that the larger a fracture zone is, the less stiff it may be and the more disposed to shearing it tends to be. Guided by the scarce data found in literature (see e.g. /Li, 1986/, Rice, 1980/ and Walsh, 1971/) and following the notion stated, the values given in Table 5-9 were assigned to the three different categories of fracture zones as input data for the 3DEC model.

Table 5-9. Properties assigned to the three categories of fractures.

	Kn, GPa/m	Ks, GPa/m	Friction angle º
Most extended	0.01	0.005	15
Less extended	0.1	0.05	20
Least extended	1.0	0.5	25

An exception was made in assigning a friction angle of 15º to the water-bearing fracture zone NNW4, i.e. the same value as was used for the same fracture zone in HQ3 analysis. The underlying idea here was the fact that the abundance of water in a fracture zone (fracture swarm) can considerably reduce the frictional resistance of that fracture zone against shearing.

Figure 5-21 shows a vertical section running E-W, on which the shear displacements along the fracture zones are depicted.

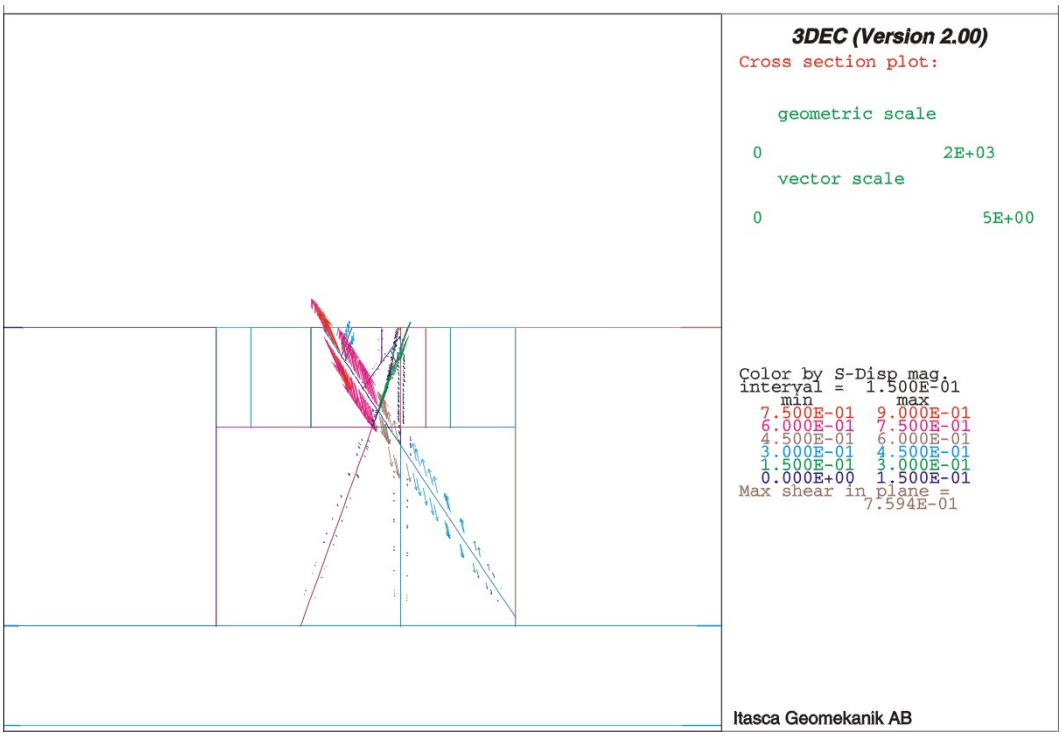

Figure 5-21. *Shear displacements along the fracture zones on a vertical section running N-S.*

Figure 5-22 shows a horizontal section at – 455-meter depth. Note that arrows indicating the direction of shearing are not occurring in plane; they are plotted in a 3D sense.

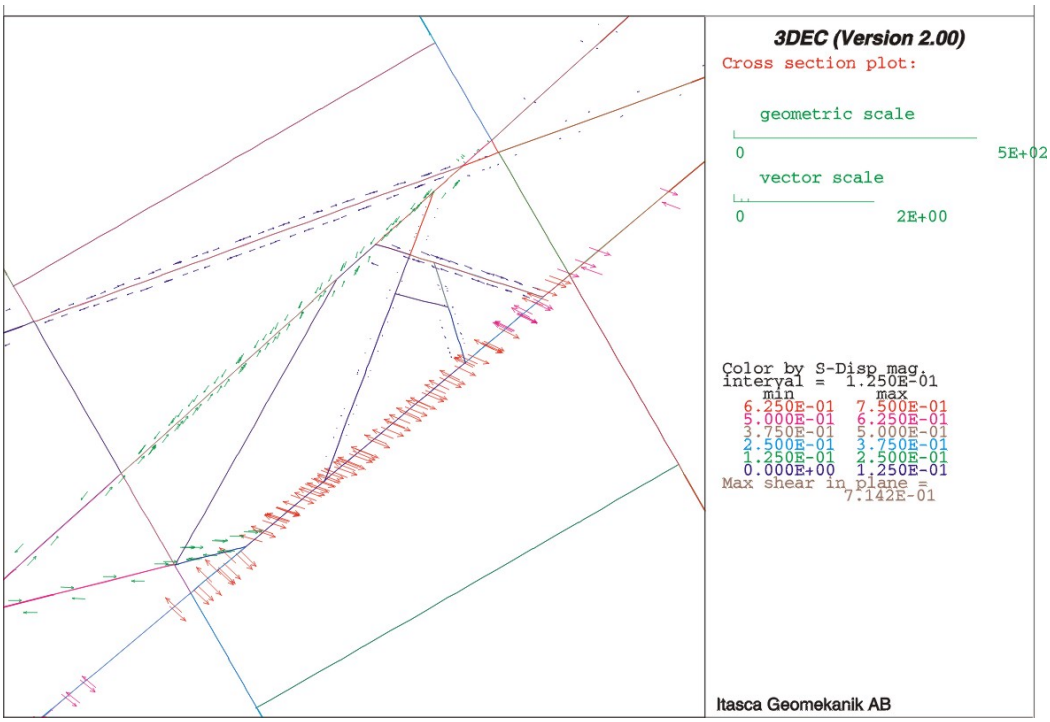

Figure 5-22. *Shear displacement along fracture zones depicted on a horizontal section at –455m depth.*

As discussed earlier, principal stresses vary as their trajectories cut across fracture zones. The variations, which include changes in magnitude, trend and plunge for a given principal stress may be most clearly shown on horizontal sections.

Two scanlines, Profile 1 and Profile 2, were chosen on a 455-meter deep horizontal section, along which the principal stresses were sampled at a number of points. Data collected included the magnitude, the trend and the plunge of each stress sampled.

Figure 5-23 shows the position of the scanlines; they were chosen to run parallel with the initial direction of the major principal stress σ_1.

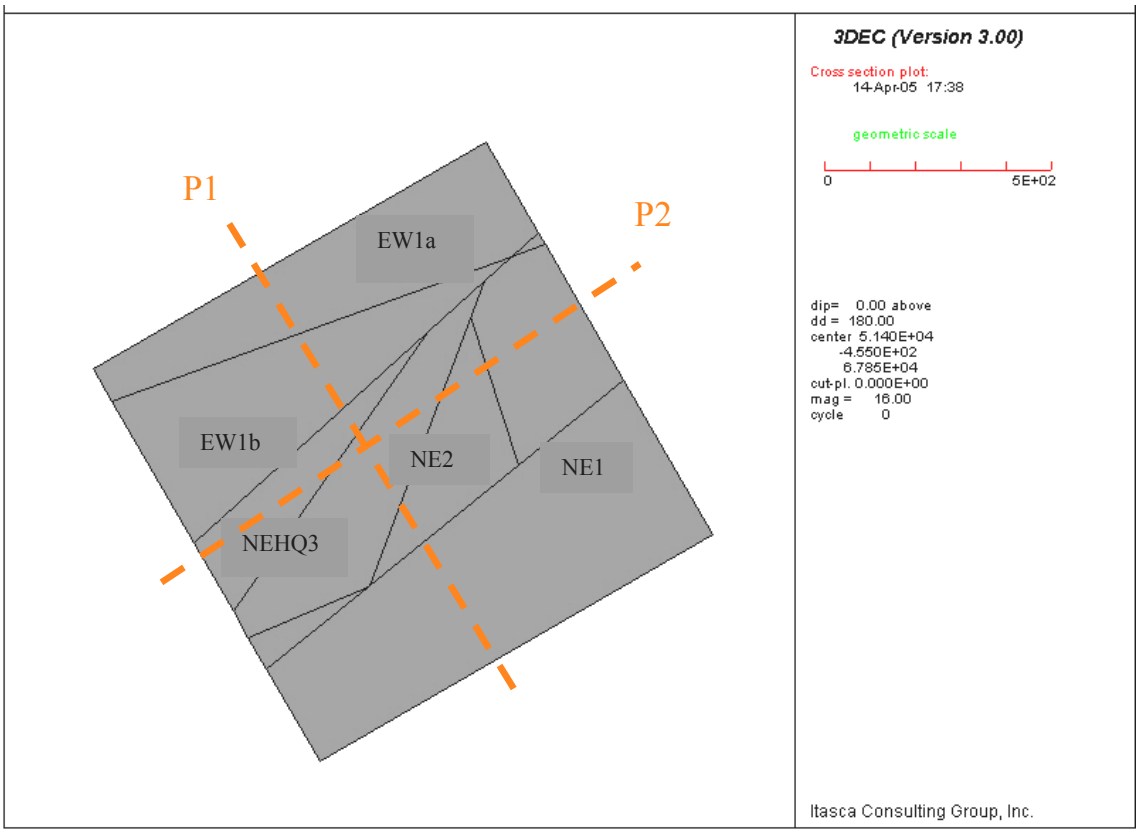

Figure 5-23. *The position of the two scanlines chosen on the horizontal section at –455 m depth, along which stress data were sampled.*

Figure 5-24 shows the variation of principal stresses, σ_1, σ_2, and σ_3, along Profile 1.

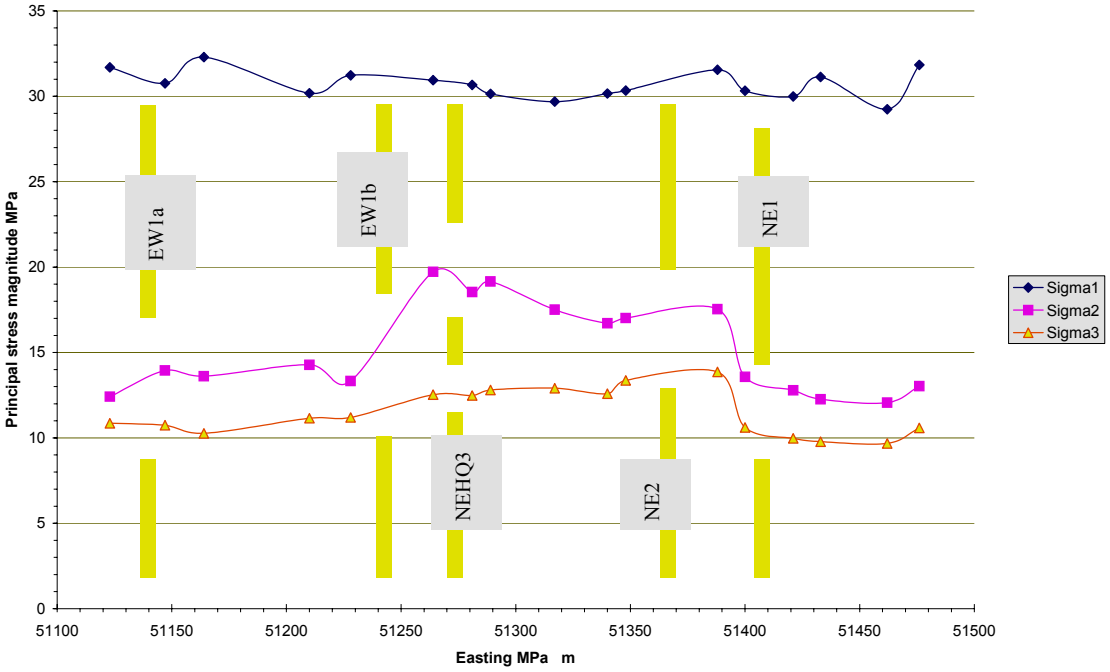

Figure 5-24. *The variation of the magnitudes of the principal stresses along Profile 1, lying across a horizontal section at – 455 m depth.*

Figure 5-25 and Figure 5-26 show the variation of the plunge and the trend of the principal stresses respectively. Note that the trend magnitudes over 180º were truncated by 180º degrees in order to get all the magnitudes in the range of 0-180º.

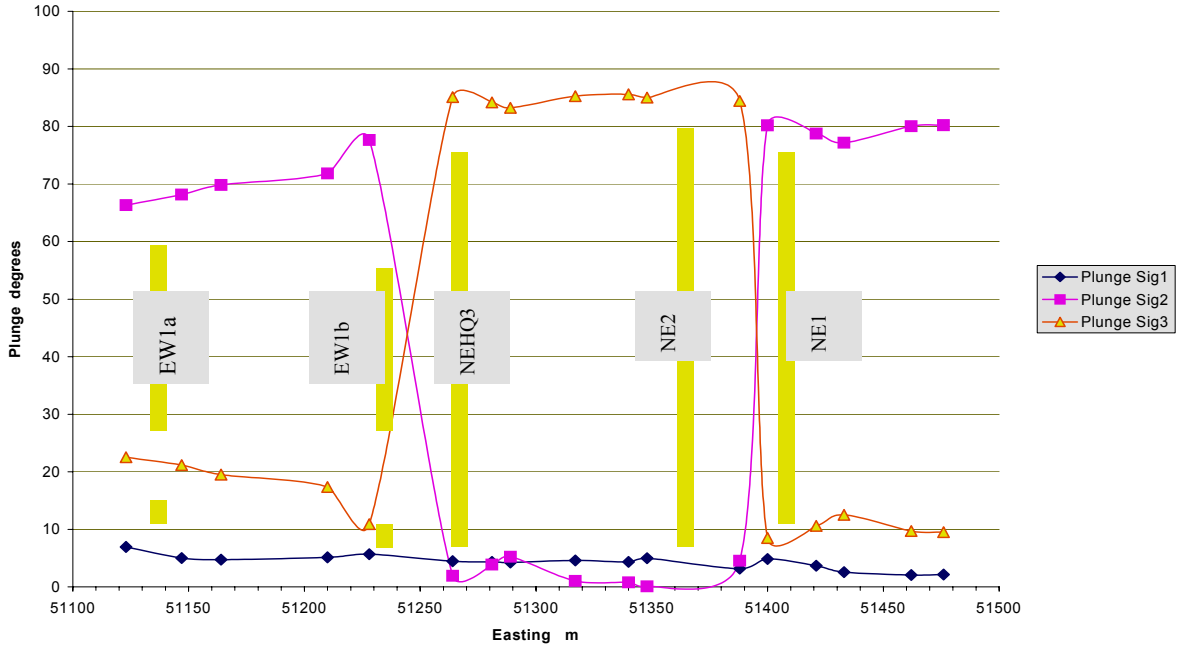

Figure 5-25*. The variation of the Plunge of the principal stresses along Profile 1, lying across a horizontal section at – 455 m depth.*

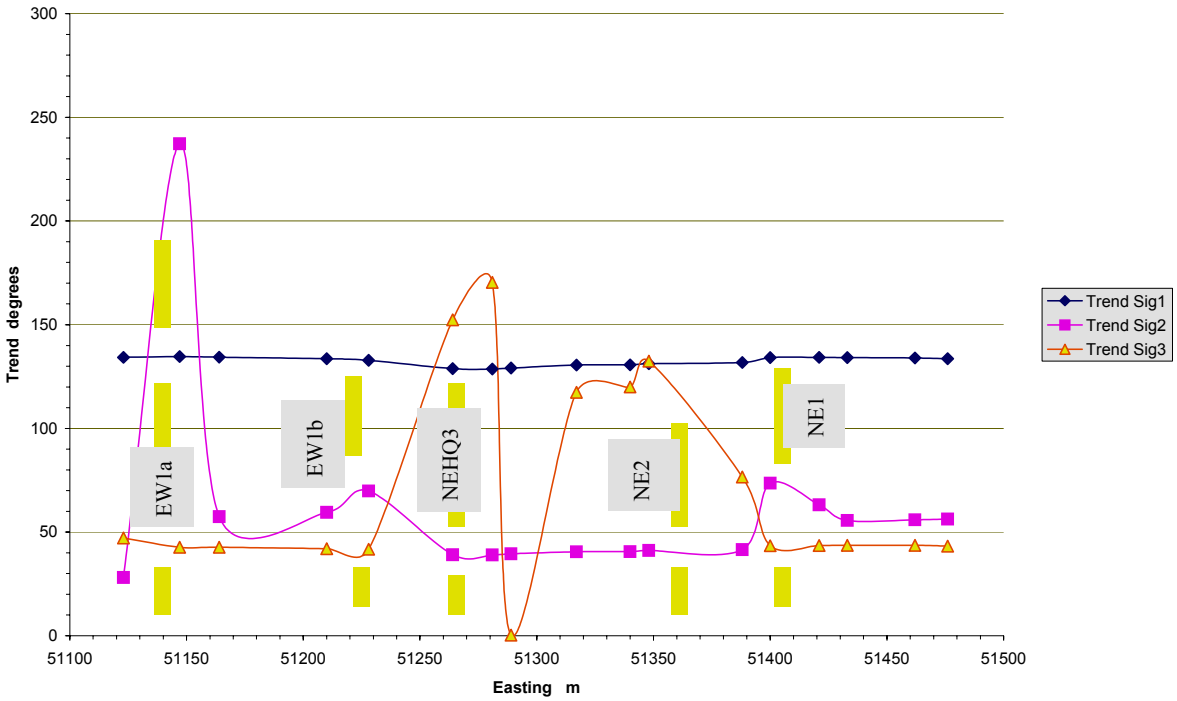

Figure 5-26. *The variation of the trend of the principal stresses along Profile 1, lying across a horizontal section at – 455 m depth.*

Figures 5-27, 5-28 and 5-29 show the variation of the principal stresses in terms of magnitude, Plunge and Trend as regards Profile 2.

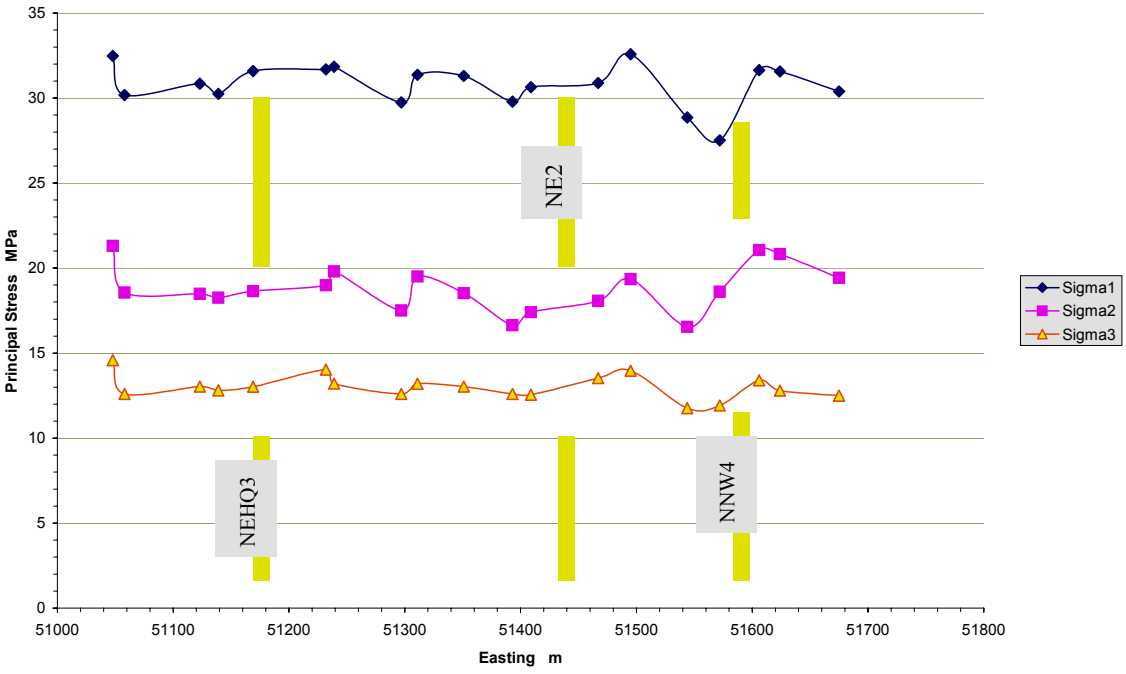

Figure 5-27. *The variation of the magnitudes of the principal stresses along Profile 2, lying across a horizontal section at – 455 m depth*

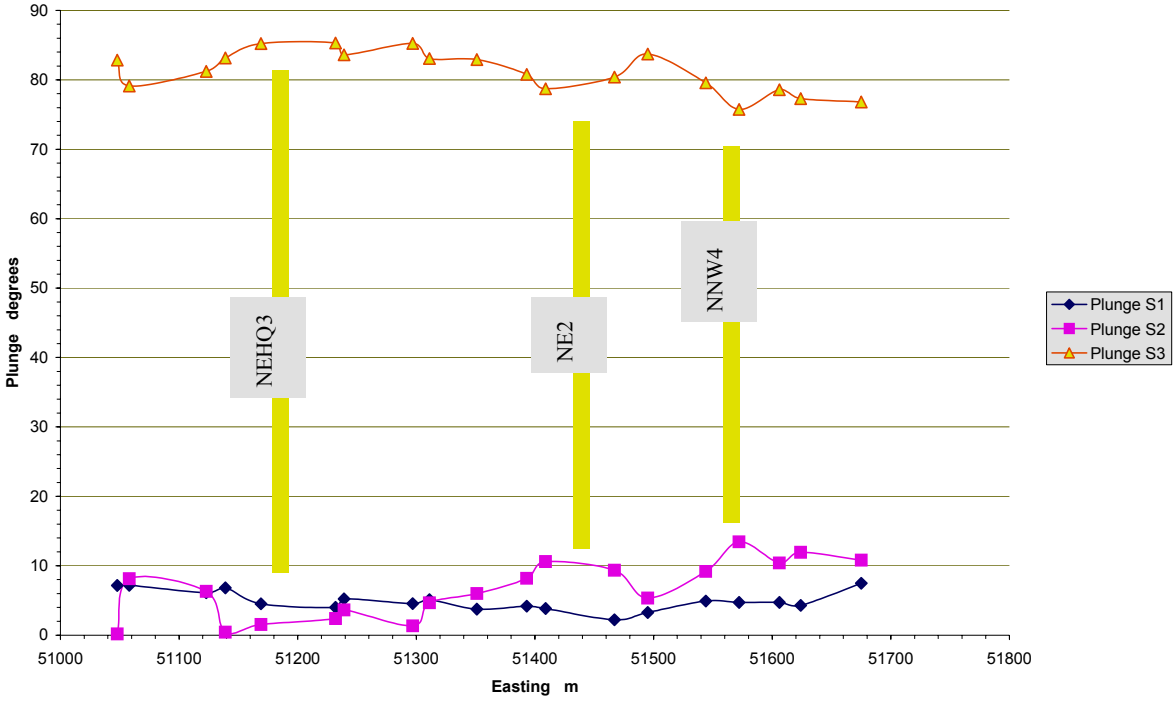

Figure 5-28. *The variation of the Plunge of the principal stresses along Profile 2, lying across a horizontal section at – 455 m depth.*

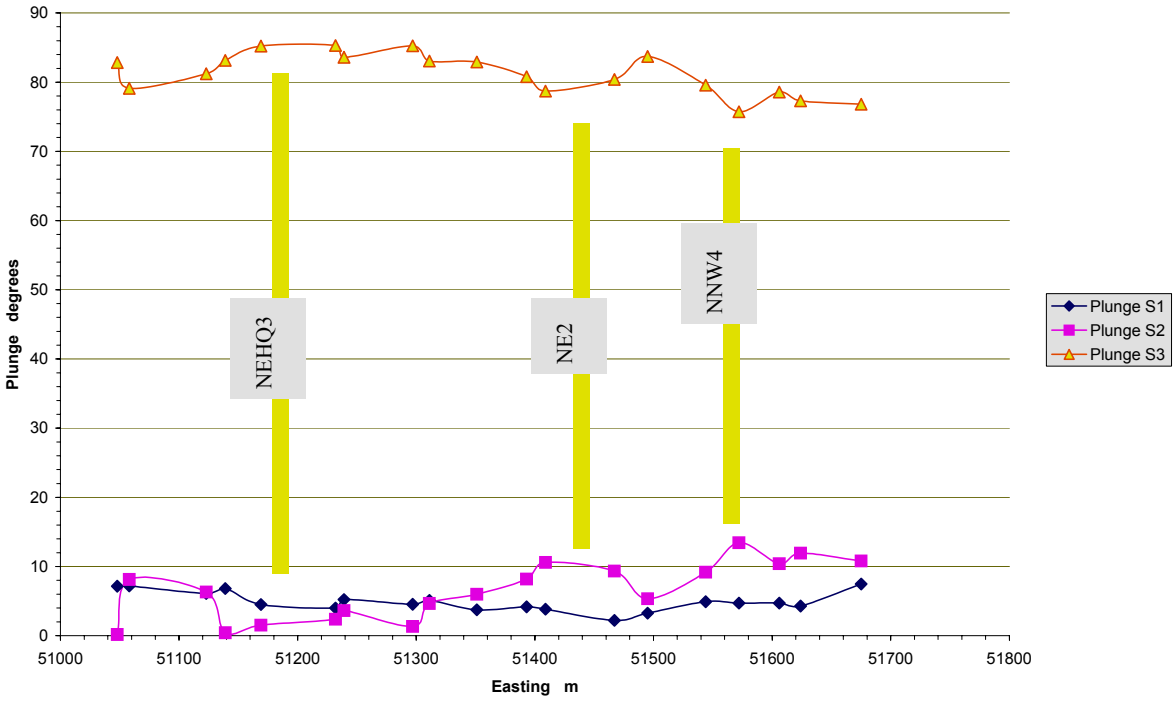

Figure 5-29*. The variation of the trend of the principal stresses along Profile 2, lying across a horizontal section at – 455 m depth.*

As can be seen, all three principal stresses vary in terms of magnitude, plunge and trend, when observed on a horizontal plane. It is difficult to find out if the variations follow a certain pattern. Note that the shearing across the fracture zones may take place in plane or out of plane, or follow any combination of those situations. As expected, the variations are more pronounced closer to the major discontinuities and are insignificant farther away from those. What could be said with a high degree of certainty is that the orientation of the major principal stress, σ_1, varies just to a limited extent, even though the point of observation would be located close to a major fracture zone. The most pronounced variation, however, takes place in the "σ_2 - σ_3 "- plane. In wedge-shaped rock parties, occurring in between major fracture zones, the variation in plunge of the two stress components can be so high that σ_2 and σ_3 can replace each other.

5.4.1 Depth-related narrowing of the fracture zones and its effect on stress distribution

Supported by the mechanics of fracture propagation within a solid, there has been much evidence from structure geological investigations that large sub vertical fracture zones; if not arrested by more dominant crossways-running fracture zones; gradually taper off with depth before they are virtually terminated within the surrounding rock mass. Information on where a considerable tapering takes place along a fracture zone, however, is difficult to obtain as it requires extensive site investigations that includes detailed seismic studies as well as sinking of quite a large number of deep boreholes which in most cases is not viable economically.

Mechanically considered, it is conceivable that the narrower portion of a fracture zone possesses different mechanical properties compared with the upper portion. As a consequence the lower portion behaves differently once it is exposed to re-activated tectonic forces.

Based on the concept mentioned and the fact that the continued structure geological investigations within the Äspö area has indeed revealed that at least the overall thickness of two fracture zones studied taper off with depth, it was decided to conduct a 3DEC analysis, in which the effect of including fracture zones with narrower sections on the distribution of the in-situ stress be studied.

In order to implement the notions given above, a conceptual model for a fracture zone was defined as follows:

- The overall thickness of steeply dipping fracture zones commonly found within igneous rock masses taper off with depth.
- The narrower section of such fracture zone is stiffer than the upper part.
- The core of the fracture zone tends to be less altered /weakened, and grows more competent with depth.

These notions were implemented into the 3DEC model for the fracture zones by:

- Choosing larger magnitudes for both normal and shear stiffness for the narrower part of a fracture zone in question
- Designating a larger value of friction angle along the narrower section of that fracture zone.

Figure 5-30 is a schematic view of a sub-vertical fracture zone showing the core and the outline of the zone of influence. A stiffer lower section is capable of transferring higher normal stress across the fracture zone and is hence less prone to shearing.

The procedure for selecting the fracture zones that were made stiffer over the deeper portion was as follows:

- In case the continued structure geological investigations confirmed that the overall thickness of a fracture zone tapered off towards deeper sections and that the fracture zone actually terminated within the limits of investigations, the fracture zone in question was made stiffer. Fracture zones NE2 and NNW4 belong to this category and were made stiffer below a depth of –400 m.
- Through going fracture zones that are extended in the 3DEC model to a depth of –3 kilometres were made stiffer below depths ranging from about -1000 to -1400m down to –3000 m. Fracture zones NE1, EW1b and EW1a belong to this category.
- The stiffness characteristics for the fracture zones EW3, HQ3, NW2 and NW1 remained unchanged over their entire extension. The through-going fracture zones NE1, EW1b and EW1a arrest these fracture zones. No information on whether their thickness taper off was available.

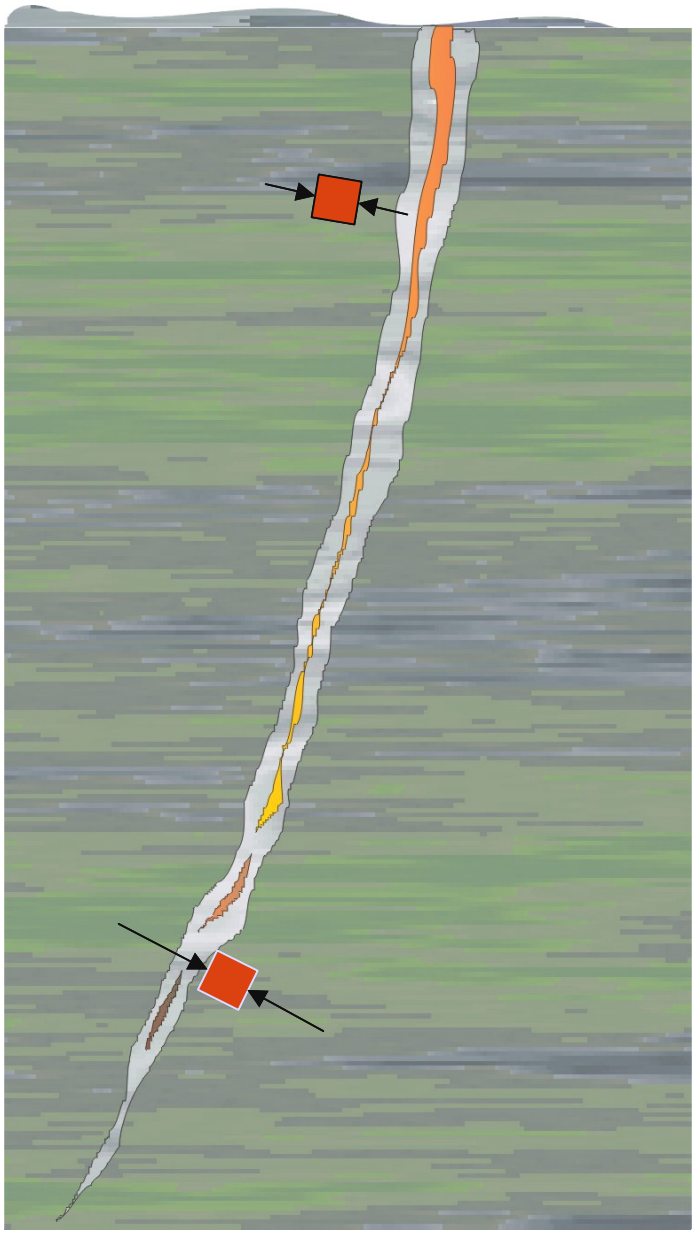

Figure 5-30*. Schematic view of a fracture zone, its core and the zone of influence, tapering off towards the deep end. Because of the lower portion being stiffer, the fracture zone is less prone to shearing over that section.*

In Table 5-10 the properties pertaining to the narrower portion of the selected fracture zones, which were used as input parameters in the 3DEC analysis, are given. The values may be compared with the corresponding values pertaining to the upper portion of the fracture zones in the same table.

Table 5-10. The input parameters for both the upper and the lower portions of the five fracture zones, which were made stiffer towards the deep end.

Fracture Zone	Input parameter for the narrower portion of the fracture zone			Input parameter for the upper portion of the fracture zone		
	Kn GPa	*Ks GPa*	*Friction angle*	*Kn GPa/m*	*Ks Gpa/m*	*Friction angle*
NE1, EW1b	0.1	0.05	25	0.01	0.005	15
EW1a	1	0.5	30	0.1	0.05	20
NE2	10	5	35	1.0	0.5	25

The results from the 3DEC analysis conducted may be best illustrated in comparison with those from the base case described in section 5.4.8. The base case may here be named as Case A and the new analysis as case B. Figure 5-31 shows an E-W running vertical section, passing through the centre of the model block in Case A. As an example, it may be noticed that the shearing occurs along the entire extension of the fracture zone NE1, though with diminishing magnitudes of shear displacements towards the deep end. This is to compare with the results from case B, Figure 5-29, where shear displacement along fracture zone NE1 almost abruptly reached small magnitudes around the depth of 1000 m.

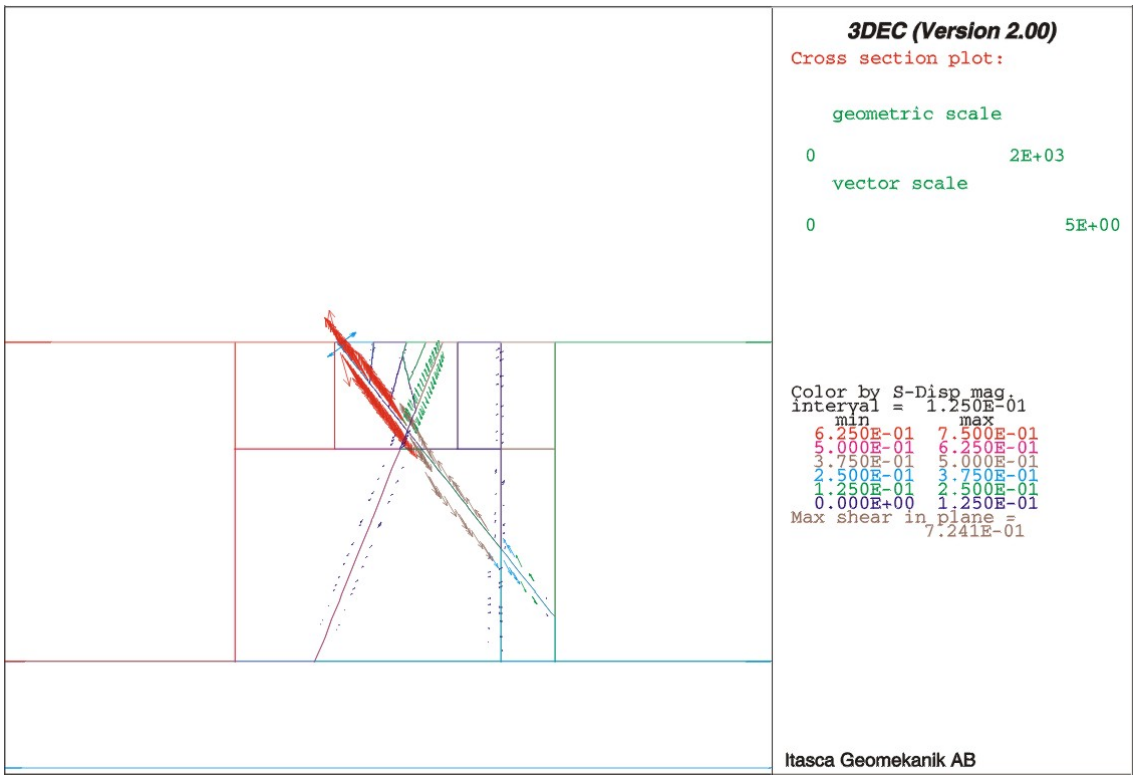

Figure 5-31*. Shear displacements along fracture zones on vertical E-W section (case A). The shear displacement magnitudes are to be compared with those shown on Figure 5-32.*

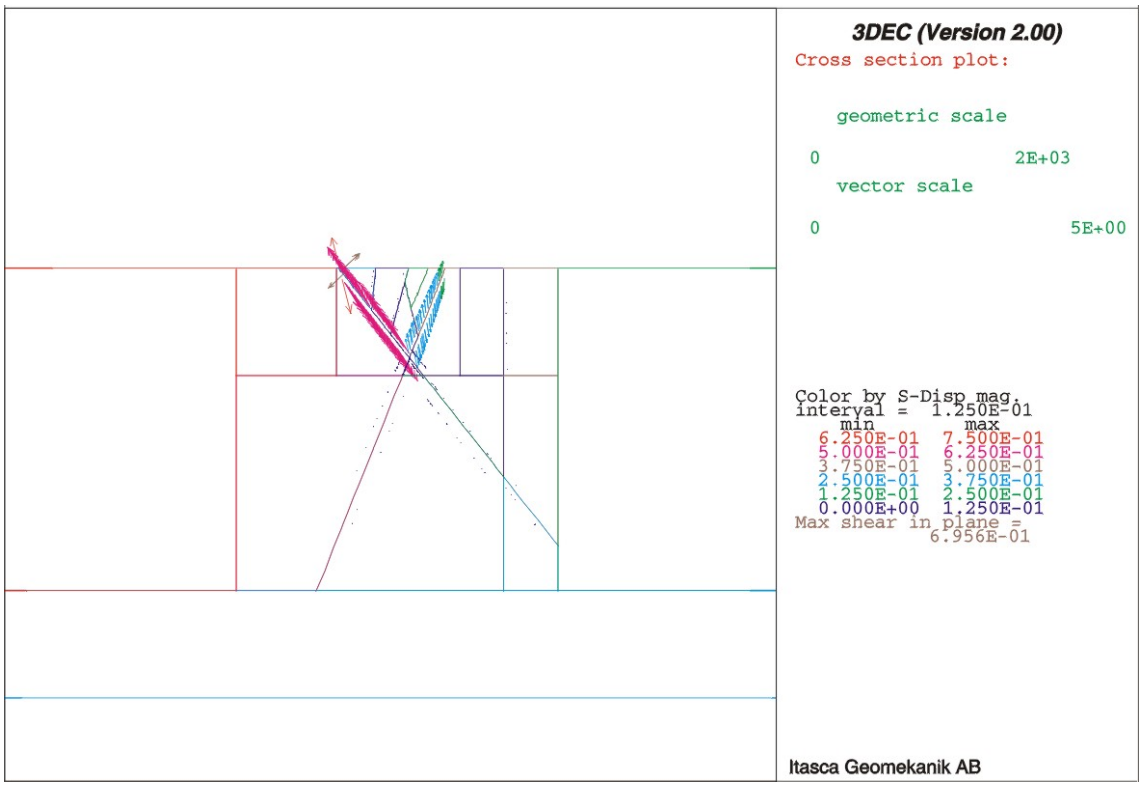

***Figure 5-32**. Shear displacements along fracture zones on vertical E-W section (Case B). The shear displacement magnitudes are to be compared with those shown on Figure 5-31.*

Figure 5-33 and Figure 5-34 show the same difference in shearing behaviour of the fracture zone NE2 from the two cases. In these two figures a comparison may be made between the shear displacement contours on the plane of the fracture zone NE2 from case A (Figure 5-33) and those from the Case B (Figure 5-34), where the shear displacement shows considerable decreasing, particularly around the deepest part of the fracture zone.

Another way of illustrating the differences between the two cases A and B was to collect the values of the principal stresses along, for example, the vertical centre line of the model block. Figure 5-35 compares the magnitudes of the major principal stress, σ_1, from case A and B. It could be seen that, with increasing depths from about 700 m, the magnitude of the σ_1 grows slightly more for Case B. This is indeed an indication that the rock mass, now having in part stiffer inclusions, is in general capable of sustaining higher magnitudes of stresses at comparable depths, as also suggested by in-situ stress measurement results. The effect is more pronounced for both σ_2 and σ_3 as could be seen on Figure 5-36 and Figure 5-37.

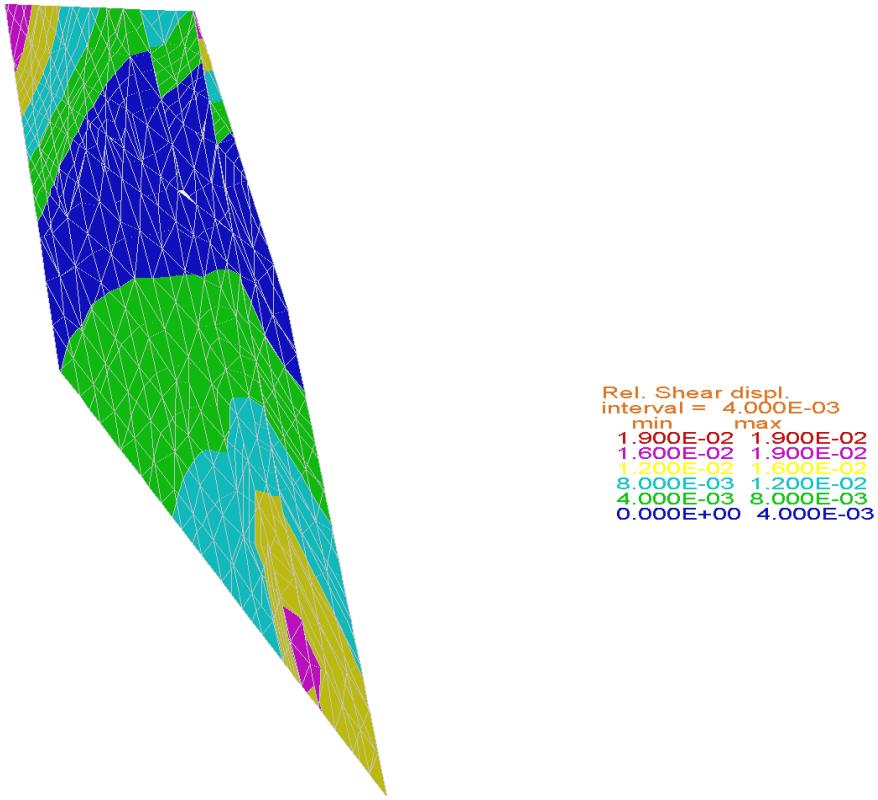

***Figure 5-33**. Shear displacement contours on fracture zone NE2 (case A). The contours are to be compared with those given in Figure 5-34.*

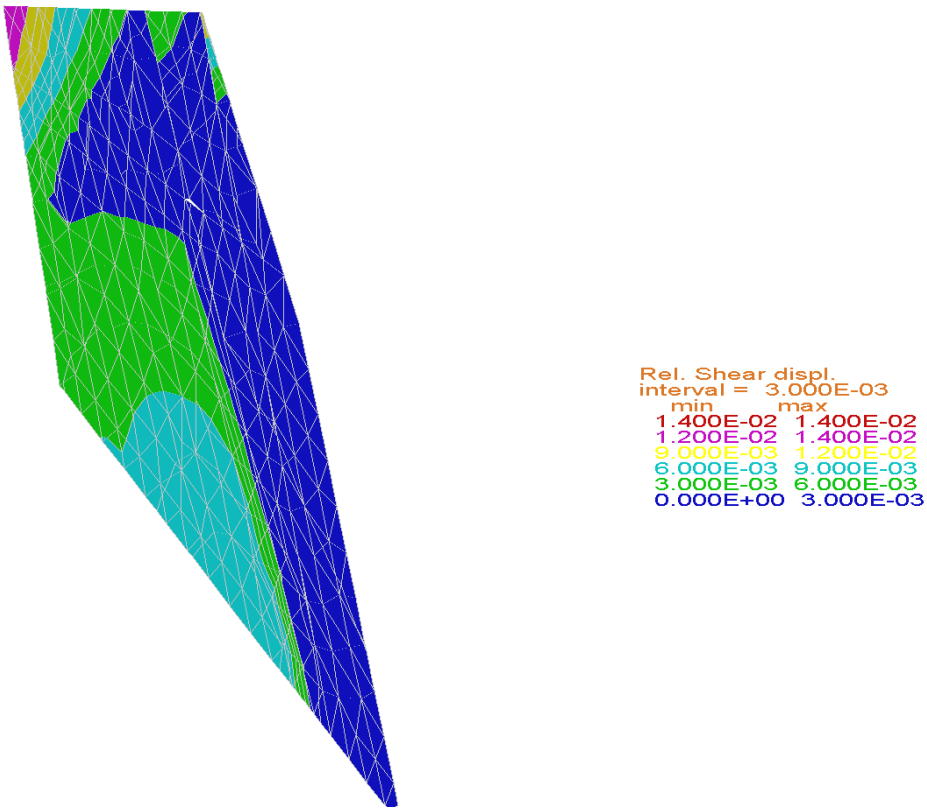

***Figure 5-34**. Shear displacement contours on fracture zone NE2 (Case B). The contours are to be compared with those given in Figure 5-33.*

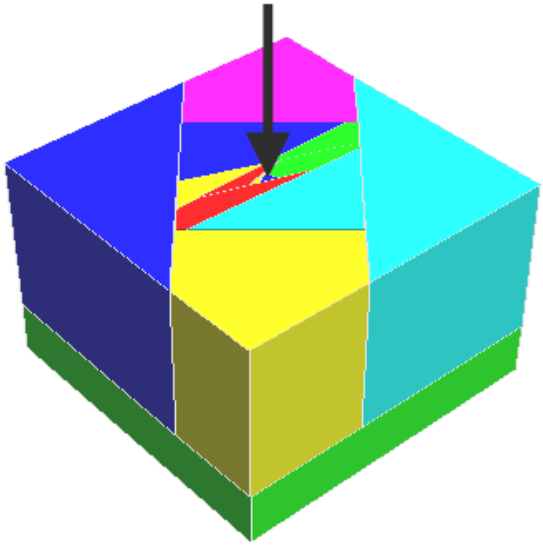

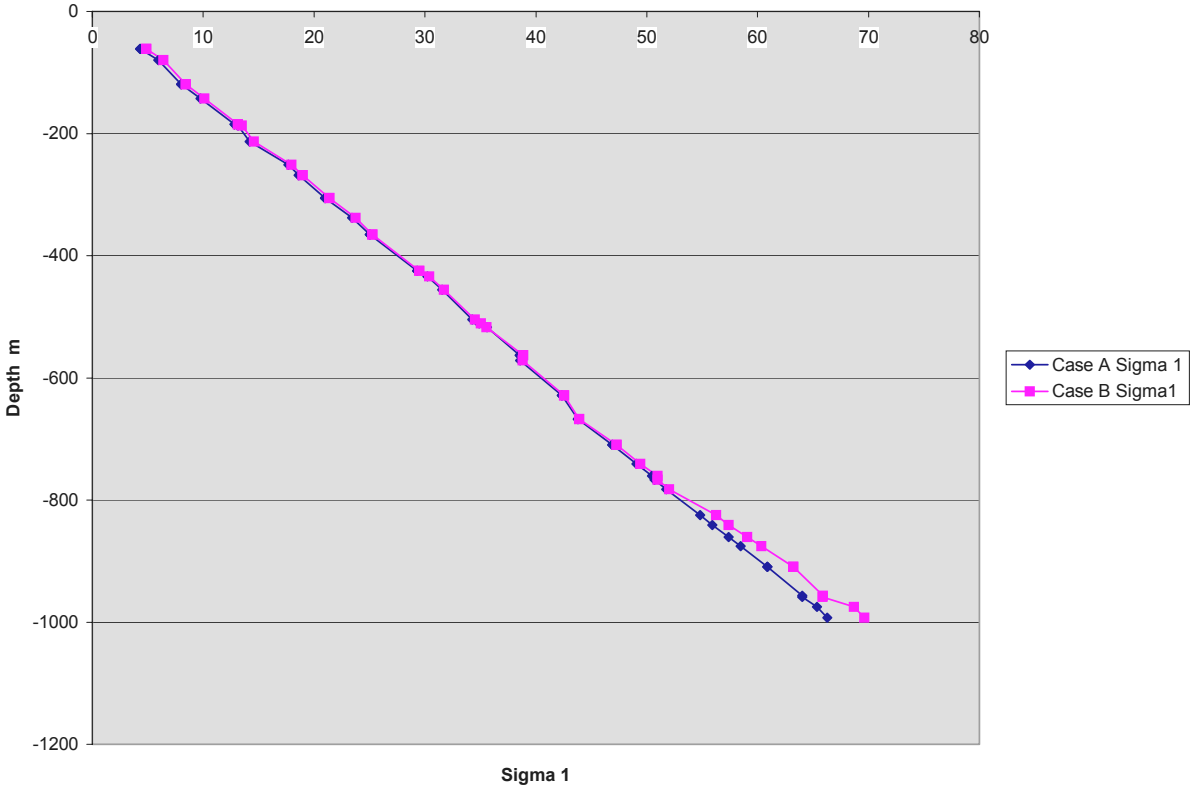

Figure 5-35. *The Variation of the major principal stress, σ1, with depth for cases A and B. In Case B, σ1 begins to slightly deviate from that belonging to Case A at about –700 m depth.*

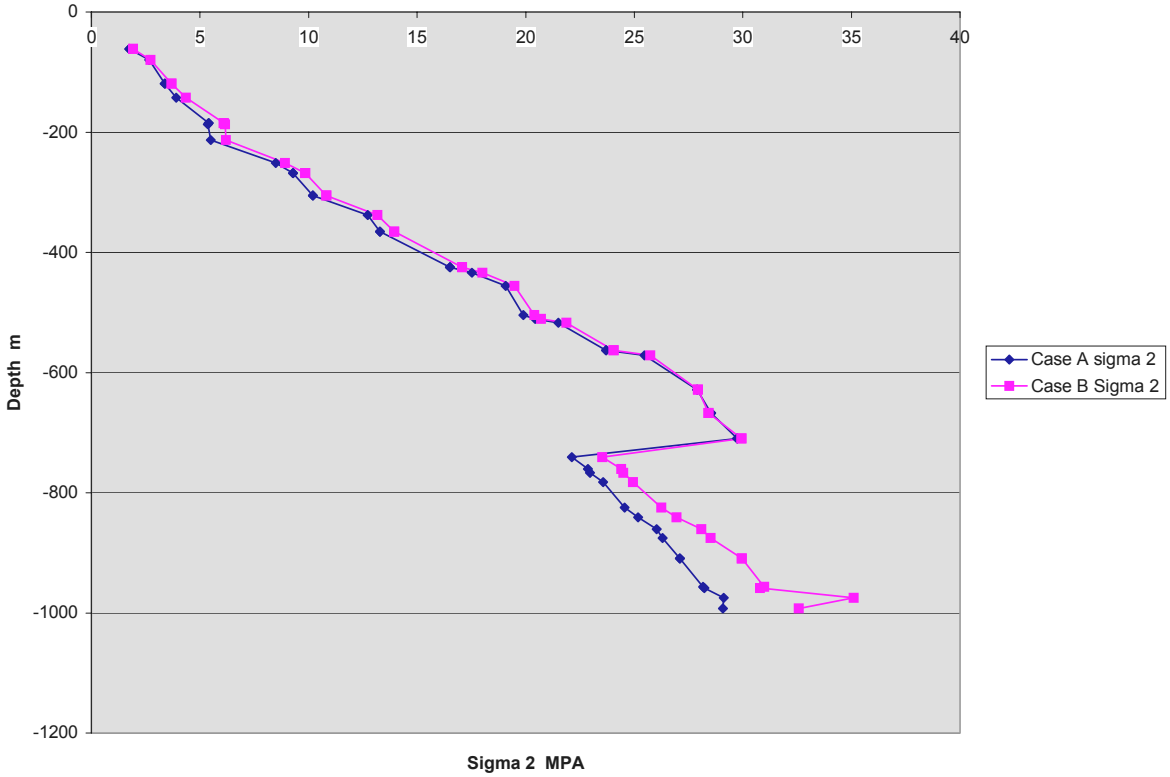

***Figure 5-36**. The variation of σ_2 with depth for Case A and Case B.*

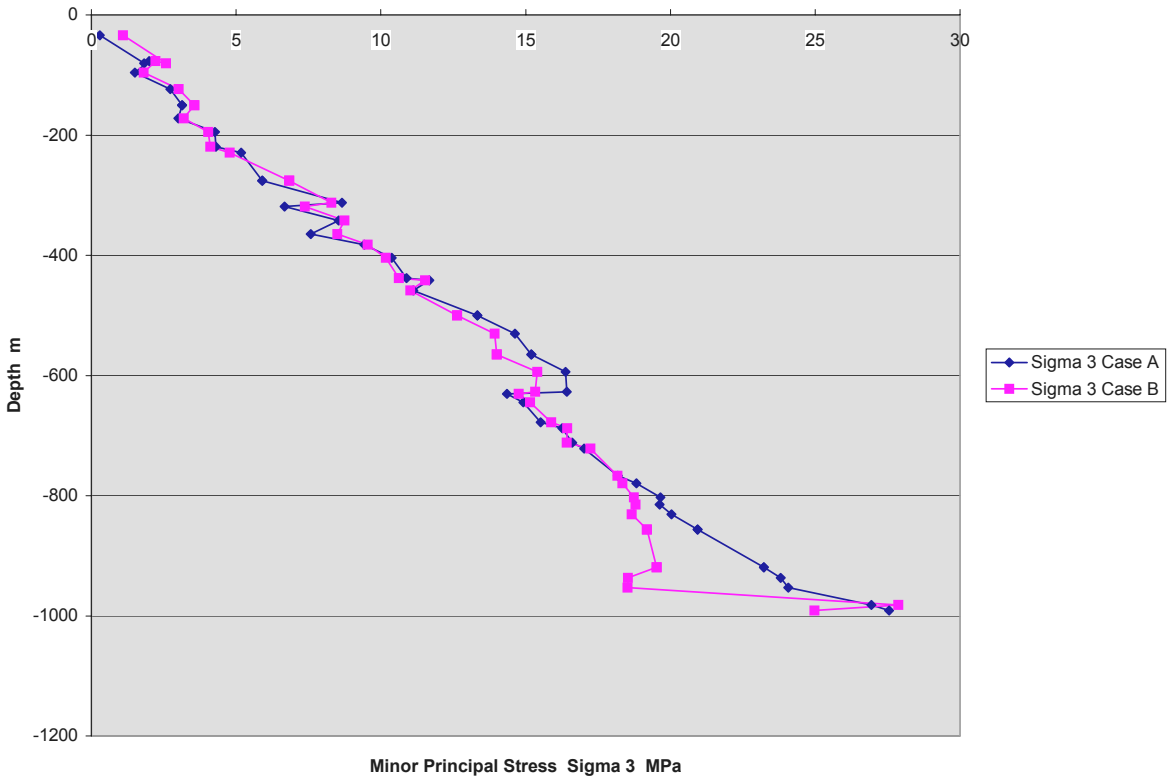

***Figure 5-37.** The variation of $\sigma 3$ with depth for Case A and Case B.*

6 The Äspö HRL site descriptive model

6.1 Rock mechanics description

6.1.1 Rock mass characterization

As was mentioned in Chapter 4, the recent investigations carried out by /Röshoff and Lanaro, 2002 and Stuab et al., 2002/ were broad and no further updating of those works was deemed necessary. Being both empirical and numerical in nature respectively, the investigations mentioned provide models describing the rock masses covering the Äspö area comprehensively.

6.1.2 Spatial distribution of principal stresses

Based on the 3DEC analyses performed it is possible to collect the main components of the stress data into a framework, which may hereinafter be called the in-situ stress model. The ultimate aim of the model would be to yield information on the spatial distribution of the in-situ stress, within a delimited rock volume, selected as a candidate to contain a repository.

The stress model should, however, be structured in such a way that it can readily be updated should new data / measurement results become available.

The geometrical data structure for the model consists of an orthogonal grid in three dimensions, where a set of data on the principal stresses are stored at the nodal points of the grid and may be retrieved when needed. A typical grid is shown in Figure 6-1.

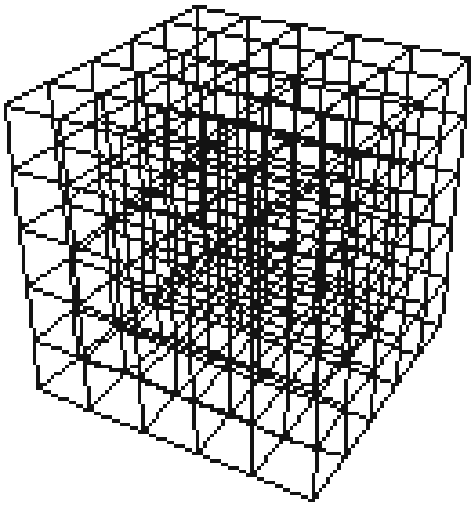

Figure 6-1. *A typical grid for storing and retrieving the stress data.*

The output of the model is a 3 dimensional illustration of the magnitudes of the principal stresses stored at the nodes of geometrical data structure, complemented by the same data in table form, given on a spreadsheet program like Excel.

The Microstation based RVS program is the tool SKB uses for visualization of findings from a number of geoscientific disciplines, including structure geology, hydrogeology, geochemistry and rock mechanics. Stress data in table form produced through a 3DEC analysis may be exported into RVS program and visualized.

Stress data may be visualized solely, or as one layer in a multi layer structure. The other layers may contain information from other disciplines, the geometry of the planned tunnel systems and / or the layout of the repository.

The following figures are examples on how in-situ stress magnitudes may be illustrated. The data set is collected from the GeoMod area and stored in a coarse grid. Figure 6-2 shows the stresses at selected points.

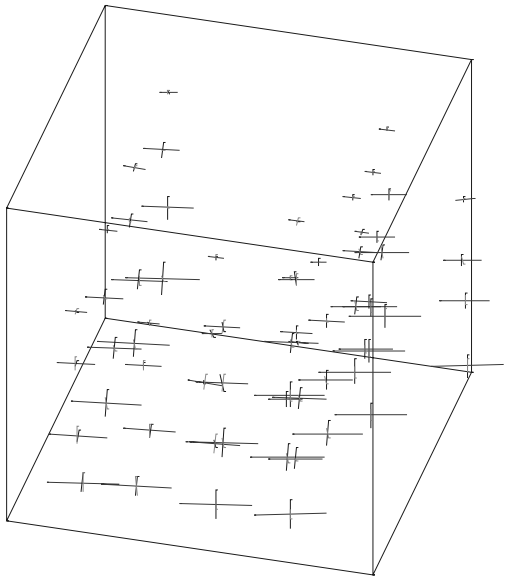

Figure 6-2. *The principal stresses illustrated at selected points within the GeoMod area*

In Figure 6-3 the tunnel system at Äspö was added to the view.

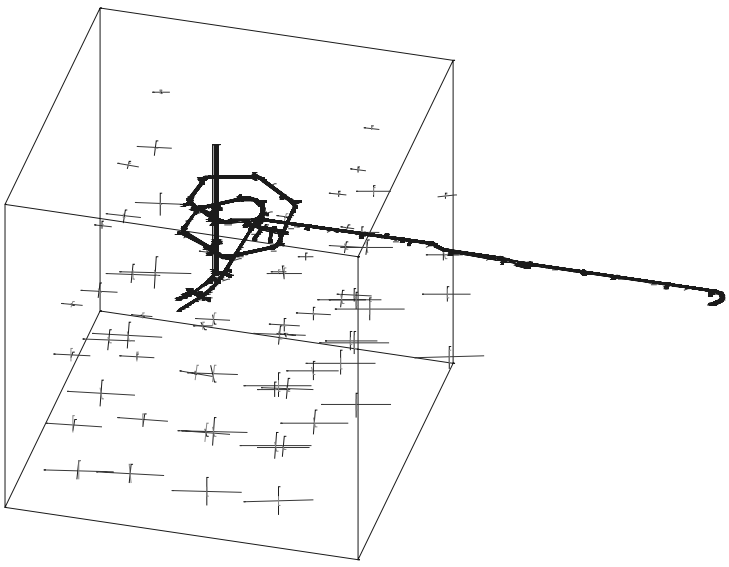

Figure 6-3. *A perspective view of the tunnel system at Äspö added to Figure 6.2.*

Figure 6-4 also includes the layout of those regional and major fracture zones, which were incorporated in the 3DEC analyses of GeoMod area.

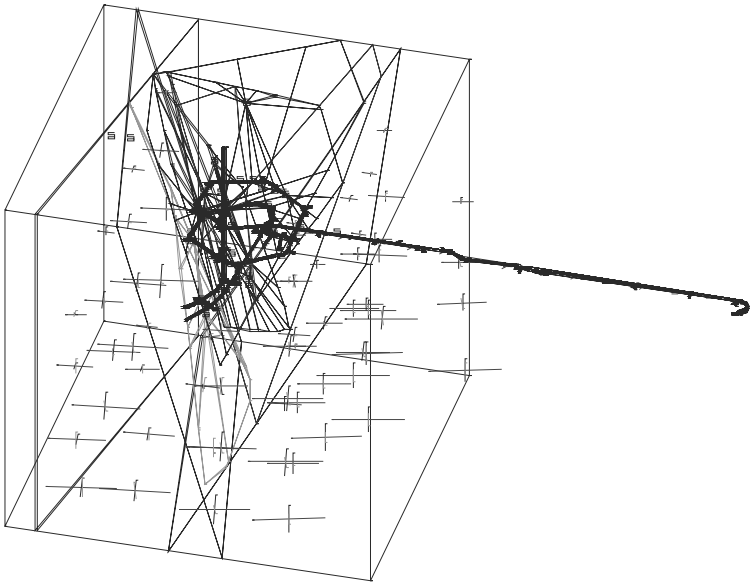

Figure 6-4. *A perspective view of the GeoMod area, including the layout of the fracture zone as modelled, the tunnel system and the principal stresses indicated by cross bars.*

The principal stresses, their plunge and trend, which formed the data set for the above illustrations are given in Table 6-1. The coloured fields indicate that any sub-set of the data set may be chosen – depending on the need - to use in conjunction with repository layout design or comparative studies. For instance the end user may wish to be ware of the major principal stress and its orientation (trend), just at a depth of approximately 515m (the highlighted field in red) or to work with all principal stress magnitudes and their orientation, which fall inside a certain thickness of the rock (highlighted field in orange).

Table 6-1. The data set including the principal stresses together with their plunge (α) and trend (β) and the coordinate of the gridpoint at each the stresses are computed.

X m	Z m	Y m	σ_1 MPa	α °	γ °	σ_2 MPa	α °	γ °	σ_3 MPa	α °	γ °
5.08E+04	-2.22E+02	6.78E+04	1.61E+01	6.23E+00	1.31E+02	7.40E+00	2.07E+01	3.81E+01	5.51E+00	6.83E+01	2.36E+02
5.11E+04	-1.93E+02	6.79E+04	1.38E+01	6.08E+00	1.36E+02	6.20E+00	5.01E+01	2.33E+02	4.78E+00	3.92E+01	4.11E+01
5.13E+04	-2.18E+02	6.81E+04	1.62E+01	8.60E+00	1.36E+02	6.20E+00	3.08E+01	2.31E+02	5.40E+00	5.78E+01	3.24E+01
5.16E+04	-2.04E+02	6.83E+04	1.44E+01	2.63E+00	1.31E+02	4.90E+00	8.45E+00	2.21E+02	3.04E+00	8.11E+01	2.35E+01
5.09E+04	-2.27E+02	6.76E+04	1.62E+01	9.66E+00	1.29E+02	1.08E+01	2.25E+01	3.53E+01	5.46E+00	6.53E+01	2.41E+02
5.12E+04	-1.86E+02	6.76E+04	1.25E+01	5.60E+00	1.38E+02	5.93E+00	6.90E+01	3.30E+01	4.66E+00	2.02E+01	2.30E+02
5.14E+04	-1.96E+02	6.76E+04	1.24E+01	8.51E+00	1.33E+02	6.39E+00	3.06E+01	3.82E+01	5.71E+00	5.80E+01	2.37E+02
5.17E+04	-1.82E+02	6.76E+04	1.11E+01	2.20E+00	1.38E+02	4.62E+00	8.56E+01	1.80E+01	2.99E+00	3.79E+00	2.28E+02
5.09E+04	-2.28E+02	6.74E+04	1.56E+01	3.87E+00	1.23E+02	1.00E+01	7.43E+00	3.21E+01	5.10E+00	8.16E+01	2.40E+02
5.13E+04	-2.05E+02	6.75E+04	1.24E+01	2.50E+00	1.30E+02	6.23E+00	7.03E+00	3.94E+01	4.22E+00	8.25E+01	2.39E+02
5.15E+04	-1.97E+02	6.75E+04	1.16E+01	3.56E+00	1.37E+02	5.01E+00	8.16E+01	2.52E+02	3.74E+00	7.60E+00	4.62E+01
5.19E+04	-2.22E+02	6.74E+04	1.39E+01	1.25E+00	3.14E+02	6.02E+00	8.87E+01	1.24E+02	4.97E+00	2.11E-01	2.24E+02
5.11E+04	-2.14E+02	6.72E+04	1.38E+01	3.01E-02	3.22E+02	7.01E+00	5.72E+01	5.19E+01	2.85E+00	3.28E+01	2.32E+02
5.13E+04	-1.98E+02	6.75E+04	1.16E+01	1.80E+00	1.33E+02	6.41E+00	4.60E+01	2.25E+02	4.95E+00	4.39E+01	4.15E+01
5.16E+04	-2.05E+02	6.76E+04	1.30E+01	3.85E+00	1.37E+02	5.47E+00	8.58E+01	3.41E+02	3.74E+00	1.67E+00	2.28E+02
5.08E+04	-3.94E+02	6.78E+04	2.76E+01	6.28E+00	1.31E+02	1.23E+01	5.61E+01	3.16E+01	1.13E+01	3.32E+01	2.25E+02
5.11E+04	-4.22E+02	6.80E+04	2.87E+01	4.62E+00	1.34E+02	1.25E+01	6.89E+01	2.36E+02	1.02E+01	2.05E+01	4.20E+01
5.13E+04	-3.91E+02	6.81E+04	2.75E+01	7.16E+00	1.34E+02	1.06E+01	7.00E+01	2.44E+02	9.76E+00	1.85E+01	4.17E+01
5.16E+04	-3.88E+02	6.83E+04	2.73E+01	5.11E+00	1.34E+02	1.21E+01	5.70E+01	2.32E+02	8.94E+00	3.25E+01	4.10E+01
5.09E+04	-3.74E+02	6.76E+04	2.59E+01	5.67E+00	1.31E+02	1.13E+01	5.93E+01	3.15E+01	7.88E+00	3.01E+01	2.24E+02
5.12E+04	-4.06E+02	6.76E+04	2.71E+01	6.52E+00	1.30E+02	1.48E+01	4.66E+00	3.90E+01	1.13E+01	8.20E+01	2.74E+02
5.15E+04	-4.00E+02	6.76E+04	2.75E+01	2.06E+00	1.30E+02	1.59E+01	4.47E+00	2.20E+02	1.25E+01	8.51E+01	1.52E+01
5.17E+04	-4.02E+02	6.76E+04	2.64E+01	2.46E+00	1.34E+02	1.09E+01	8.75E+01	3.07E+02	8.68E+00	3.24E-01	4.40E+01
5.09E+04	-3.95E+02	6.75E+04	2.64E+01	8.56E+00	1.38E+02	1.59E+01	2.39E+01	4.43E+01	1.16E+01	6.45E+01	2.47E+02
5.13E+04	-3.91E+02	6.75E+04	2.50E+01	4.57E+00	1.35E+02	1.07E+01	7.09E+01	2.38E+02	7.33E+00	1.85E+01	4.33E+01
5.15E+04	-4.13E+02	6.74E+04	2.71E+01	1.51E+00	1.34E+02	1.10E+01	8.15E+01	2.34E+02	9.00E+00	8.31E+00	4.39E+01
5.18E+04	-4.23E+02	6.74E+04	2.81E+01	1.46E-01	1.33E+02	1.13E+01	8.79E+01	2.27E+02	9.58E+00	2.08E+00	4.33E+01
5.10E+04	-3.98E+02	6.73E+04	2.56E+01	4.56E+00	1.34E+02	1.14E+01	5.63E+01	2.30E+02	8.11E+00	3.33E+01	4.05E+01
5.14E+04	-4.01E+02	6.74E+04	2.61E+01	2.50E+00	1.34E+02	1.10E+01	7.47E+01	2.34E+02	8.61E+00	1.51E+01	4.37E+01
5.17E+04	-3.95E+02	6.76E+04	2.62E+01	3.46E+00	1.34E+02	1.09E+01	8.55E+01	2.74E+02	8.60E+00	2.90E+00	4.42E+01
5.19E+04	-4.10E+02	6.78E+04	2.69E+01	2.88E+00	1.35E+02	1.12E+01	8.46E+01	1.22E+01	8.77E+00	4.52E+00	2.25E+02
5.08E+04	-6.39E+02	6.78E+04	4.34E+01	5.42E+00	1.32E+02	1.82E+01	6.22E+01	3.19E+01	1.53E+01	2.72E+01	2.25E+02
5.11E+04	-6.03E+02	6.79E+04	4.06E+01	4.51E+00	1.33E+02	1.72E+01	7.49E+01	2.40E+02	1.41E+01	1.44E+01	4.22E+01
5.14E+04	-6.01E+02	6.81E+04	4.10E+01	5.63E+00	1.33E+02	1.67E+01	7.82E+01	2.52E+02	1.47E+01	1.03E+01	4.23E+01
5.16E+04	-5.86E+02	6.83E+04	4.01E+01	4.56E+00	1.33E+02	1.78E+01	6.12E+01	2.31E+02	1.37E+01	2.84E+01	4.03E+01
5.09E+04	-5.83E+02	6.76E+04	3.91E+01	5.45E+00	1.32E+02	1.78E+01	7.02E+01	2.70E+01	1.29E+01	1.90E+01	2.24E+02
5.12E+04	-5.95E+02	6.76E+04	3.96E+01	5.71E+00	1.30E+02	2.53E+01	1.62E+00	3.94E+01	1.66E+01	8.41E+01	2.94E+02
5.14E+04	-6.03E+02	6.76E+04	4.01E+01	3.52E+00	1.33E+02	1.74E+01	8.25E+01	2.51E+02	1.36E+01	6.66E+00	4.30E+01
5.09E+04	-5.80E+02	6.74E+04	3.84E+01	5.36E+00	1.33E+02	2.41E+01	1.87E+01	4.11E+01	1.63E+01	7.05E+01	2.38E+02
5.13E+04	-6.12E+02	6.74E+04	4.13E+01	2.71E+00	1.33E+02	1.76E+01	7.74E+01	2.35E+02	1.39E+01	1.23E+01	4.25E+01
5.15E+04	-6.01E+02	6.75E+04	4.02E+01	1.59E+00	1.33E+02	1.66E+01	8.47E+01	2.41E+02	1.35E+01	5.04E+00	4.29E+01
5.10E+04	-5.94E+02	6.72E+04	3.96E+01	2.33E+00	1.33E+02	1.70E+01	7.20E+01	2.30E+02	1.35E+01	1.78E+01	4.18E+01
5.14E+04	-5.95E+02	6.74E+04	3.99E+01	1.99E+00	1.33E+02	1.66E+01	7.84E+01	2.33E+02	1.33E+01	1.14E+01	4.26E+01
5.16E+04	-5.61E+02	6.76E+04	3.73E+01	2.08E+00	1.33E+02	1.56E+01	8.61E+01	2.55E+02	1.24E+01	3.30E+00	4.30E+01
5.19E+04	-6.01E+02	6.78E+04	4.01E+01	1.72E+00	1.34E+02	1.63E+01	8.56E+01	2.07E+01	1.30E+01	4.04E+00	2.24E+02
5.08E+04	-7.94E+02	6.77E+04	5.35E+01	4.56E+00	1.33E+02	2.36E+01	7.48E+01	2.56E+01	1.90E+01	1.44E+01	2.24E+02
5.11E+04	-7.78E+02	6.80E+04	5.20E+01	4.27E+00	1.33E+02	2.31E+01	8.04E+01	2.49E+02	1.85E+01	8.64E+00	4.25E+01
5.13E+04	-8.07E+02	6.81E+04	5.42E+01	5.03E+00	1.33E+02	2.27E+01	7.65E+01	2.45E+02	1.92E+01	1.25E+01	4.20E+01

7 Conclusions

The fact that a detailed structure geological characterization of the HQ3 area was available lent itself well to performing numerical analyses that would reveal the contribution of local geological structures on stress distribution. Site investigations in virgin areas, i.e. where no underground opening exists, provide merely information on regional and major discontinuities.

Details such as the presence of water in geological structures, the beginning and the termination point of a fracture / fracture zone, the thickness of a fracture / fracture zone and like wise help attributing more plausible parameters to those structures when included in a numerical model. This was the case when analyzing the HQ3 area. As an example, the fact that the fracture swarm, partly found in that area, is water-filled justifies that a comparatively lower friction coefficient be attributed to that structure.

The numerical analyses with the focus on the so-called GeoMod area were enhanced in steps, along with the progress that was made on the structure geological investigations during the course of this project. New features were incorporated as soon as they were made adequately known. The flexibility, built in the numerical grid, proved to be functional in that it could readily accommodate the new changes.

The major principal stress, σ_1, in general, is considered as the most influential factor controlling, among others, the flow through rock fractures, tendency for emergence of new fractures, opening and closure of fractures. Also much attention is paid to the orientation of the major principal stress when an underground facility is designed. This study tends to show that the orientation of σ_1 does not deviate much along its stress trajectories, even though the point of observation lies close to a major fracture zone.

The main variation of stress tensor occurs in the "σ_2 - σ_3 "- plane, where the rotation of the two principal stresses can be so high that σ_2 and σ_3 replace each other within a certain depth interval.

References

Amadei B, StepHansen O, 1997. Rock Stress and its Measurement. Chapman & Hall.

Hakami E, Hakami H, Cosgrove J, 2002. Strategy for a Rock Mechanics Site descriptive Model. Development and testing of an approach to modelling the state of stress. SKB R-02-03. Svensk Kärnbränslehantering AB.

Itasca, 1998. User manuals, 3DEC – Three dimensional Distinct Element Code. Itasca Consulting group Inc., Minneapolis, Minnesota.

Lundholm B, 2000. Äspö Hard Rock Laboratory-Rock stress and rock stress measurementat ÄspöHRL. SKB IPR-00-24. Svensk Kärnbränslehantering AB.

Röshoff K, lanaro F, Lanru J, 2002. Strategy for a Rock Mechanics Site descriptive Model. Development and testing of the empirical approach. SKB R-02-01. Svensk Kärnbränslehantering AB.

Staub I, Fredriksson A, Outters N, 2002. Strategy for a Rock Mechanics Site descriptive Model. Development and testing of the theoretical approach. SKB R-02-02. Svensk Kärnbränslehantering AB.

Andersson J, Christiansson R, Hudson JA, 2002. Site investigation strategy for development of a rock mechanics site descriptive model. SKB TR-02-01. Svensk Kärnbränslehantering AB.

Rice J R, 1980. The mechanics of earthquake rupture. In physics of the Earth Interior, edited by Dziewonski and E. Boschi, Italian Physical society, Bologna, Italy. Pp555-649.

Walsh, J B, 1971. Stiffness in Faulting and in Friction Experiments. Journal of Geophysical research, No 35, Vol 76.

Li, Victor C, 1986. Mechanics of shear rupture applied to earthquake zones. Fracture Mechanics of Rock, Editor B. Atkinson, Academic press Inc.

Hansen L M, Hermansson J, 2002. Äspö Hard rock Laboratory, Local model of geological structures close to the TASF-tunnel. SKB international Progress Report IPR-02-15.